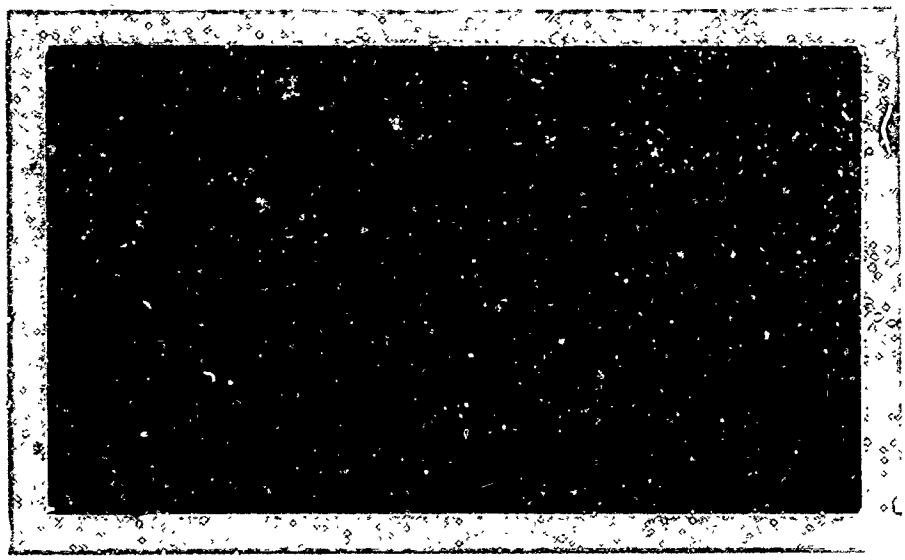

DREXEL INSTITUTE OF TECHNOLOGY

DREXEL INSTITUTE OF TECHNOLOGY

Wave Propagation Research Center

Philadelphia, Pennsylvania

Report 125-12

CALCULATIONS OF EXPANDING SHOCK WAVES

AND

LATE-STAGE EQUIVALENCE

Shih Lien Huang and Pei Chi Chou

April 1968

FINAL REPORT
FOR THE PERIOD AUGUST 1965 to NOVEMBER 1967

Contract No. DA-18-001-AMC-876(X)

Sponsored through the U. S. Army Ballistics Research Laboratories

Aberdeen Proving Ground, Maryland

TABLE OF CONTENTS

LIST OF FIGURES

ABSTRACT

A numerical scheme of the method of characteristics, the Hartree scheme, is developed to calculate the flow field of the expansion of a high pressure sphere into atmosphere. The accuracy of this scheme in solving one dimensional fluid problems is evaluated by applying it to the blast wave problem for which the exact solution can readily be calculated to a high degree of accuracy. It is shown that this method is very accurate, involving errors of less than 1%. In calculating the expanding sphere, two rather challenging problems, namely, the initial singularity and the formation of a second shock, are successfully solved through special techniques.

The propagation of the expanding main shock and the propagation of the contact surface which separates the ambient fluid from the fluid initially confined in the high pressure sphere are accurately determined.

The formation of an inward traveling shock, or the second shock to distinguish it from the main shock, from the previously continuous flow field is found to exist at the tail of the left traveling rarefaction wave. Though the strength of the second shock remains rather weak at the early stage of its development, it grows rapidly to very high strength just before it implodes on the center of the sphere. The path of the second shock in the physical plane is accurately defined and some interesting behavior of the second shock is revealed.

Based on accurate detailed numerical calculations by the Hartree scheme, it is shown that "late-stage equivalence" exists in the expansion of high pressure spheres into atmosphere, provided the initial total energy in each of the spheres is held constant. Late-stage equivalence is assumed to exist if the peak pressure distribution for different expanding spheres are the same for long times. Moreover, if the initial masses enclosed in each sphere are also kept the same in addition to constant initial energy, late-stage equivalence exists not only for peak pressure of the main shock, but also for the positions of both the main shock and the second shock in the physical plane.

NOMENCLATURE

c = speed of sound

c_1 = constant speed of sound outside wave zone

c_p = specific heat at constant pressure

c_v = specific heat at constant volume

E = parameter proportional to the total energy within the wave

E_o = initial total energy released

H = enthalpy per unit mass

K = constant

P_o = initial pressure of the high pressure sphere

P = pressure

P_1 = constant pressure outside wave zone

S = entropy per unit mass

t = time variable

T = absolute temperature

u = particle velocity

U = shock wave velocity

x = space variable

x_o = initial radius of the high pressure sphere

γ = specific heat ratio

ρ = density

ρ_o = initial density of the high pressure sphere

ρ_1 = constant density outside wave zone

ϵ = length expressing energy and pressure scaling ($\epsilon^3 = \frac{E_o}{P_1}$)

λ = energy reduced radial distance ($\frac{x}{\epsilon}$)

τ = energy reduced time ($\frac{c_1 t}{\epsilon}$)

I INTRODUCTION

Ever since the discovery of explosives people have been interested in the behavior of explosions. Today, considerable attention is still focused on the gas-dynamics of explosions. It is very difficult, if not impossible, to represent the actual situation in the initial stage for a real explosion which involves chemical reactions, detonation waves, combustion or nuclear reactions. However, after the initial stage, the situation is essentially the expansion of a high pressure sphere. Even this problem of expanding gas has no exact solution. Simplified models as well as various numerical calculations have been used to study the problem in the past.

The most well-known simplified model is the point source solution; while among the numerical calculations the finite-difference method and method of characteristics are widely adopted.

1. Point Source

In the so-called point source model it is assumed that a finite amount of energy in an infinitely concentrated form is being released suddenly into the atmosphere. The solution of this ideal model will be referred to as the point source solution in later discussions.

In the point source solutions of Taylor (1) and Sedov (2) the properties of the flow are assumed to be self-similar; the governing partial differential equations are reduced to ordinary differential equations.

Taylor integrated these equations numerically and the results were presented in tabular form while Sedov successfully integrated these ordinary equations and obtained closed form solutions. In their analyses, strong shock relations were used across the outward propagating shock front. Therefore, the solution is invalid for shock pressure somewhat below 100 atm. Besides, in real explosions the source of energy is far from being a point.

In order to extend the range of validity of the point source solution, the exact shock equations must be used whenever the influence of the atmospheric counter pressure can no longer be ignored.

To extend to low pressures Goldstine and Von Neumann (3) modified the point source solution in the range from 100 atm. to 1.017 atm. A finite-difference method was used in the calculation with initial data calculated from point source solution. Exact shock relations were used across the shock front at low pressures. Numerical results were given which can be used to compare with our calculation.

Brode (4) also extended the point source solution in the range of 1,600 atm. to 1.06 atm. with a finite-difference method. However, Brode used the artificial viscosity method in handling the shock discontinuity. Since this particular method always has to spread the shock discontinuity across several grid zones, the shock front cannot be clearly defined.

In a different approach Sakurai (5) modified the point source solution by a series expansion in y, defined by $\frac{c_o^2}{U^2}$, where c_o is the velocity of sound of the atmosphere, and U is the shock velocity. The zeroth order solution is exactly Taylor's solution. Higher order

approximations supplement Taylor's solution such that the exact shock equations are satisfied.

2. Numerical Calculations

A. Finite Difference

One of the earliest numerical calculations by the finite-difference method was by Unwin (6), who in 1941, calculated a problem starting from the sudden release of a spherically symmetric flow in a compressible medium, having constant entropy everywhere, into the atmosphere. The initial density distribution is so defined such that no shock will be formed. Results are not applicable to the general case where shocks are involved.

Roberts (7) used the finite-difference method developed by P. D. Lax to calculate the same problem treated by Unwin. Lax's finite-difference scheme introduces a viscous effect which tends to smooth out discontinuities in the flow variables when they arise. Since we expect a second shock which will be formed in the expanding gas for our problem, therefore, it is reasonable to assume this method will not yield satisfactory results.

The attenuation of spherical shock at large distance from the origin is investigated by Whitham (8). As an approximation, the flow is assumed to be isentropic in his analysis. He showed that for a weak explosion, behind the shock front an envelope of characteristics is formed and hence a second shock must appear.

To handle hydrodynamic problems which involve shock discontinuities, Von Neumann and Richtmyer (9) developed a numerical method. In applying

this method, an artificial viscosity is introduced, and shocks are smeared out so that the mathematical surfaces of discontinuity are replaced by layers of thickness comparable to several meshes. Therefore, there is a lack of definition of the solution. Brode (4) applied this method to calculate the spherical wave produced by sudden release of high pressure gas into the atmosphere to very late times. Due to the nature of the method, which cannot handle the initial singularity at the outer boundary, Brode's results are inaccurate even at the early stage. One of his calculations with high initial gas density, the overpressure vs radius curve presented in his paper is grossly inaccurate.

B. Method of Characteristics

Since the method of characteristics will give correct treatment of singularities such as centered rarefactions and shock discontinuities, it generally leads to better defined boundaries and more accurate results.

Wecken (10) calculated, by the standard method of characteristics, the spherical wave produced by an expansion of a high pressure gas sphere. Based on numerical grounds he predicated the existence of an inward traveling second shock, which travels toward the inside relative to the moving gas. It will be reflected at $r = 0$ and then travel outward behind the main shock. Employing the same method, Wecken obtained numerical solution for the explosion originated from detonation of a spherical charge, and the results were used to compare experimental measurements obtained by Schardin (11). Although results showed overall

agreement between experimental and numerical calculations, Schardin considered Wecken's calculations lack accuracy, and recommended further calculations by digital computer.

The standard method of characteristics was also used to calculate the problem treated by Unwin (6) by Fox and Ralston (12). Constant entropy everywhere was assumed in the formulation. Therefore, their solutions are restricted to problems where no shock discontinuities are present.

In 1960, Zhukov (13) using the standard method of characteristics calculated a problem of sudden release of a constant pressure sphere into vacuum. Outside the expanding sphere, a spherical envelope of fluid exists. The primary interest of this problem is the interaction of the main shock and the outer fluid shell. The second shock was formed as a result of intersection of characteristics of one family (II Characteristics). After its formation the second shock was calculated for only a short time. Details of the numerical scheme or results were not presented.

An alternative numerical scheme of method of characteristics was proposed by Hartree (14). He suggested integrating equations of motion along characteristic directions but instead of using the characteristic grid, using a given interval in one independent variable. It may give the results in a more desirable form, particularly if the one independent variable happens to be time. This method has the advantage of yielding results at a specific time, whereas if the results are obtained on a grid of characteristics, lengthy interpolation is required to obtain

such results. Besides, the Hartree scheme gives results along particle paths thus making it particularly advantageous in handling problems with contact discontinuities.

Hoskin (15) discussed Hartree's scheme in great detail, but no specific example was presented to demonstrate its application.

Lister (16) followed essentially Hartree's proposal and devised a numerical scheme, geared to digital computer computation, which can be applied only to isentropic flow.

Katshova and Chuskin (17) developed a numerical scheme, similar to the Hartree scheme, suitable for computer calculations of steady axisymmetric supersonic flows of perfect gas with shock wave. Their numerical results were in good agreement with those by standard method of characteristics.

It seems that, up to the present, the Hartree scheme has not been applied to unsteady flow problems involving shock waves and entropy change.

One of the difficulties in the solution of the expansion of a high pressure sphere is the initial singularity at the boundary. In general, an outward moving shock, a contact discontinuity surface, and a centered rarefaction wave are formed instantaneously. Unwin (6), Roberts (7) and Fox (12) avoid these difficulties by requiring the initial distribution of density to be a particular function of radius, and assuming entropy to be constant everywhere.

McFadden (18) obtained a solution for short times after the release of a uniform high pressure sphere. Flow properties u, c, and S (entropy)

were developed in powers of γ, which is proportional to time. Solutions up to the first order were derived which satisfy the boundary conditions to the first order without introducing a second shock. As he suggested, we have computed the example given in his paper, and find that our results are in good agreement with McFadden's.

The mathematical nature of the singularity of the disturbance due to the detonation of a spherical charge initiated at the center was investigated by Berry and Holt (19). The equations of unsteady spherical motion are solved in the neighborhood of the singularity at the origin of the air blast wave in the t-x plane. Expansions are used in series of half-powers of r, the radial distance from origin, with coefficients θ depending on the transverse coordinate.

Two singular characteristics are found to start at the origin. One is the left traveling characteristic in the rarefaction wave region and the other is the contact discontinuity surface. Near these lines the expansions are invalid. To remove these difficulties, Berry and Holt (19) used the Paincare-Lighthill-Kou method by introducing a new independent variable z and expanded the dependent variables (u, p, c) and the independent variable (θ and ξ) in series of power of ξ with coefficients depending on z.

This is equivalen. to a perturbation of coordinates θ . The development of the second shock was investigated and asserted to be an effect of at least second order of ξ .

The results from the series expansion were used as initial data to determine the early development of the growth of spherical blast from a

particular charge. Berry et al (20) integrated the equations of motion along characteristics. Results of the calculation are crude. They were content with an accuracy adequate for plot only.

3. Late-Stage Equivalence

It was suggested by many authors (Taylor, Brode, Sakurai, Courant and Friedrichs, etc.) that real explosions, though they behave differently in the early stage, gradually become equivalent if the initial energies are equal. Among these who suggested such a late-stage equivalence, Sakurai (5) made a very strong statement that the point source model, although not adequate to represent a real explosion in the early stage, becomes more and more accurate at the late stages, regardless of the kind of explosives or the features of the explosives. The assumption of late-stage equivalence intuitively seems plausible. However, it has not been verified. Brodé (4) calculated a few cases of the releasing of high pressure spheres into the atmosphere and tried to indicate that the pressure behind the main shock front approaches the corresponding point source solution in late stages. Unfortunately due to the limitation of the numerical method used in his calculation, results were inaccurate even at the early stage.

4. Outline of the report

It is the intention of this report first to develop a numerical scheme which is accurate, and can be easily adapted to computer calculations. This scheme is then used to calculate the flow field developed from a spherically symmetric high pressure sphere suddenly released in

the atmosphere. The existence of a late-stage equivalence will be investigated by calculating and comparing expansion of many high pressure spheres with different initial radii, pressures, and densities. Late-stage equivalence is assumed to exist if the peak pressure distributions for different expanding spheres are the same for long times.

II BASIC METHOD

1. Basic Differential Equations

The governing equations for an unsteady spherically symmetric continuous flow of polytropic gas without friction and heat transfer are the continuity equation

$$\frac{\partial \rho}{\partial t} + \rho \frac{\partial u}{\partial x} + u \frac{\partial \rho}{\partial x} + 2 \frac{\rho u}{x} = 0 \tag{2-1}$$

the momentum equation

$$\frac{\partial u}{\partial t} + u \frac{\partial u}{\partial x} + \frac{1}{\rho} \frac{\partial p}{\partial x} = 0 \tag{2-2}$$

the energy equation

$$\frac{\partial S}{\partial t} + u \frac{\partial S}{\partial x} = 0 \tag{2-3}$$

and the equation of state

$$S = S_0 + \frac{c_v}{\gamma - 1} \operatorname{Log}\left(\frac{p}{\rho^\gamma}\right) \tag{2-4}$$

where S_0 = constant

Substituting (2-4) into (2-3) yields

$$\frac{\partial}{\partial t}\left(\frac{p}{\rho^\gamma}\right) + u \frac{\partial}{\partial x}\left(\frac{p}{\rho^\gamma}\right) = 0 \tag{2-5}$$

2. Method of Characteristics and Characteristic Equations

The general theory of characteristics can be found in many books, such as Von Mises (21), Courant and Friedrichs (22). Here we will limit our discussion to the current problem which is a quasi-linear first order system of hyperbolic type with two independent variables. The essense

of the method is to search for a set of characteristic coordinates. By using these characteristic coordinates, a new system can be obtained from original partial differential equations. The differentiation of the new system will be considerably simplified. For the present case, the differentiations for each characteristic equation will be along a single characteristic coordinate. Therefore, numerical integration along a characteristic coordinate is particularly simple.

A characteristic coordinate is along the tangent of a characteristic curve which is defined as a curve on which the derivatives of the fluid properties are indeterminate.

Since we will have occasion to use the characteristic equation in plane case, the derivation will be kept in a more general form. The continuity equation becomes

$$\frac{\partial \rho}{\partial t} + \rho \frac{\partial u}{\partial x} + u \frac{\partial \rho}{\partial x} + (\nu - 1) \frac{\rho u}{x} = 0 \qquad (2\text{-}6)$$

where $\nu = 1$ for plane motion, $\nu = 2$ for cylindrical motion and $\nu = 3$ for spherical motion; the momentum equation remains as:

$$\frac{\partial u}{\partial t} + u \frac{\partial u}{\partial x} + \frac{1}{\rho} \frac{\partial p}{\partial x} = 0 \qquad (2\text{-}7)$$

and from the equation of state of a polytropic gas and the definition of sound velocity

$$c^2 = \left(\frac{\partial p}{\partial \rho} \right)_s = \gamma \frac{p}{\rho}$$

equation (2-5) can be written in the form:

$$\frac{\partial p}{\partial t} + u \frac{\partial p}{\partial x} - c^2 \left(\frac{\partial \rho}{\partial t} + u \frac{\partial \rho}{\partial x} \right) = 0 \qquad (2\text{-}8)$$

For regions where the flow properties u, p, and ρ are continuous, three equations for the total differentials du, dp, and dρ may be written. Combining these differential relations with the governing differential equations (2-6), (2-7) and (2-8) we obtain the following set of differential equations involving six partial derivatives: $\frac{\partial u}{\partial x}$, $\frac{\partial u}{\partial t}$, $\frac{\partial p}{\partial x}$, $\frac{\partial p}{\partial t}$, $\frac{\partial \rho}{\partial x}$, and $\frac{\partial \rho}{\partial t}$ which are in question for indetermination.

$$
\begin{aligned}
dx\frac{\partial u}{\partial x} + dt\frac{\partial u}{\partial t} &= du \\
dx\frac{\partial p}{\partial x} + dt\frac{\partial p}{\partial t} &= dp \\
dx\frac{\partial \rho}{\partial x} + dt\frac{\partial \rho}{\partial t} &= d\rho \\
\rho\frac{\partial u}{\partial x} + u\frac{\partial \rho}{\partial x} + \frac{\partial \rho}{\partial t} &= -(\nu-1)\frac{\rho u}{x} \\
u\frac{\partial u}{\partial x} + \frac{\partial u}{\partial t} + \frac{1}{\rho}\frac{\partial p}{\partial x} &= 0 \\
u\frac{\partial p}{\partial x} + \frac{\partial p}{\partial t} - uc^2\frac{\partial \rho}{\partial x} - c^2\frac{\partial \rho}{\partial t} &= 0
\end{aligned}
\qquad (2\text{-}9)
$$

Solving these equations for $\frac{\partial u}{\partial x}$ by Cramer's Rule, we obtain

$$
\frac{\partial u}{\partial x} = \frac{N}{D} \qquad (2\text{-}10)
$$

where

$$
D = \begin{vmatrix}
dx & dt & 0 & 0 & 0 & 0 \\
0 & 0 & dx & dt & 0 & 0 \\
0 & 0 & 0 & 0 & dx & dt \\
\rho & 0 & 0 & 0 & u & 1 \\
u & 1 & \frac{1}{\rho} & 0 & 0 & 0 \\
0 & 0 & u & 1 & -uc^2 & -c^2
\end{vmatrix}
$$

$$
= (u\,dt - dx)\left[(u+c)dt - dx\right]\left[(u-c)dt - dx\right]
$$

and

$$N = \begin{vmatrix} du & dt & 0 & 0 & 0 & 0 \\ dp & 0 & dx & dt & 0 & 0 \\ d\rho & 0 & 0 & 0 & dx & dt \\ -(\nu-1)\frac{\rho u}{x} & 0 & 0 & 0 & u & 1 \\ 0 & 1 & \frac{1}{\rho} & 0 & 0 & 0 \\ 0 & 0 & u & 1 & -uc^2 & -c^2 \end{vmatrix}$$

$$= (udt-dx)\left[(\nu-1)\frac{uc^2}{x}(dt)^2-(udt-dx)du+\frac{dp}{\rho}dt\right]$$

In order that $\frac{\partial u}{\partial x}$ to be indeterminate D must be 0. The vanishing of D produces the three physical characteristics:

I characteristic $\frac{dx}{dt} = u + c$ (2-11)

II characteristic $\frac{dx}{dt} = u - c$ (2-12)

III characteristic $\frac{dx}{dt} = u$ (2-13)

Notice that the III characteristic is a path line.

Along these physical characteristics, the derivative $\frac{\partial u}{\partial x}$ is indeterminate and therefore may be discontinuous. To insure that $\frac{\partial u}{\partial x}$ is indeterminate but not infinite, the numerator, N, of equation (2-10) must also vanish along the characteristics. Along the III characteristics, (udt - dx) = 0, N = 0 identically; the vanishing of N along the other two characteristics yields the following state characteristics, (or compatibility equations)

$$du = \mp \frac{dp}{c\rho} \mp (\nu-1)\frac{uc}{x}dt \qquad (2\text{-}14)$$

where the upper sign refers to I characteristic and the lower sign refers to II characteristic.

When equations (2-9) are solved for the other derivatives, we have:

$$\frac{\partial u}{\partial t} = \frac{1}{D}(udt-dx)\left[-(\nu-1)\frac{uc^2}{x}dxdt-(udu+\frac{dp}{\rho})dx+(u^2-c^2)dudt\right] \quad (2\text{-}15)$$

$$\frac{\partial p}{\partial x} = \frac{1}{D}(udt-dx)\left\{\left[-(\nu-1)\frac{\rho uc^2}{x}dt-dp\right](udt-dx)+\rho c^2 dudt\right\} \quad (2\text{-}16)$$

$$\frac{\partial p}{\partial t} = \frac{1}{D}(udt-dx)\left\{\left[(\nu-1)\frac{\rho uc^2}{x}dx+udp\right](udt-dx)-c^2dpdt-\rho c^2 dudx\right\} \quad (2\text{-}17)$$

The vanishing of the numerators of $\frac{\partial u}{\partial t}$, $\frac{\partial p}{\partial x}$ and $\frac{\partial p}{\partial t}$ yields results which are identical to those for $\frac{\partial u}{\partial x}$.

When equations (2-9) are solved for $\frac{\partial \rho}{\partial x}$ and $\frac{\partial \rho}{\partial t}$ we have

$$\frac{\partial \rho}{\partial x} = \frac{1}{D}\left\{(udt-dx)\left[\left(-(\nu-1)\frac{\rho u}{x}dt-d\rho\right)(udt-dx) + \rho dudt\right] + c^2 d\rho(dt)^2 - dp(dt)^2\right\} \quad (2\text{-}18)$$

$$\frac{\partial \rho}{\partial t} = \frac{1}{D}\left\{(udt-dx)\left[\left((\nu-1)\frac{\rho u}{x}dx+ud\rho\right)(udt-dx) - \rho dxdu\right] + dpdxdt - uc^2 d\rho(dt)^2\right\} \quad (2\text{-}19)$$

The vanishing of the numerators of $\frac{\partial \rho}{\partial x}$ and $\frac{\partial \rho}{\partial t}$ yields, in addition to equation (2-14), the III state characteristic

$$d\rho = \frac{1}{c^2}dp \quad (2\text{-}20)$$

It is convenient to eliminate the density ρ from the characteristic equations by the relation $c^2=\gamma\frac{p}{\rho}$. When this substitution is made, and

the III state characteristic equation integrated, the following characteristic equations, in terms of p, u, and c are obtained.

State Characteristics

$$(du)_I = -\frac{c}{\gamma p}(dp)_I - (\nu-1)\frac{uc}{x}(dt)_I \tag{2-21}$$

$$(du)_{II} = \frac{c}{\gamma p}(dp)_{II} + (\nu-1)\frac{uc}{x}(dt)_{II} \tag{2-22}$$

$$\left(\frac{p}{p^\circ}\right)_{III} = \left(\frac{c}{c^\circ}\right)_{III}^{\frac{2\gamma}{\gamma-1}} \tag{2-23}$$

The constants c° and p° must be evaluated for each III characteristic.

In the numerical procedure of the method of characteristics, all governing differential equations are put into finite-difference form. Thus, equations (2-11) to (2-13), (2-21) and (2-22) become

along I and II $$\frac{\Delta x}{\Delta t} = \bar{u} \pm \bar{c} \tag{2-24}$$

$$\Delta u = \mp \frac{\bar{c}}{\bar{p}}\left(\frac{\Delta p}{\gamma}\right) \mp (\nu-1)\left(\frac{\bar{u}\bar{c}}{\bar{x}}\right)\Delta t \tag{2-25}$$

along III $$\frac{\Delta x}{\Delta t} = \bar{u} \tag{2-26}$$

where Δ represents the difference between two adjacent points along a characteristic and the barred values represent the average between the two points. Notice that referring to the pivotal point (mesh point)

x_i, $\Delta u = u_i - u_{i-1}$ is the backward difference of u; although it is sometimes considered as the central difference at "half-way" point $x_{i+\frac{1}{2}}$.

3. Normal Shock Equations

The equations expressing the conservations of mass, momentum and energy across a moving shock are:

$$\rho_1 U = \rho_2 \left[U \pm (u_1 - u_2) \right] \tag{2-27}$$

$$p_1 + \rho_1 U^2 = p_2 + \rho_2 \left[U \pm (u_1 - u_2) \right]^2 \tag{2-28}$$

$$H_1 + \frac{U^2}{2} = H_2 + \frac{\left[U \pm (u_1 - u_2) \right]^2}{2} \tag{2-29}$$

where U is the shock velocity relative to the medium into which it moves. Subscripts 1 and 2 refer to the states ahead of and behind the shock front respectively. The upper sign applied for shocks travels to the right and the lower sign for left traveling shocks, but U is always taken as positive. To make these equations more suitable for later use, the following algebraic manipulations are in order. For polytropic gases we have

$$H = C_p T = C_p \frac{1}{R}\left(\frac{p}{\rho}\right) = \frac{C_p}{(C_p - C_v)}\left(\frac{p}{\rho}\right) = \frac{1}{\left(1 - \frac{1}{\gamma}\right)}\left(\frac{p}{\rho}\right)$$

Since

$$c^2 = \gamma\left(\frac{p}{\rho}\right)$$

therefore $$H = \frac{c^2}{\gamma - 1} \tag{2-30}$$

Using relation (2-30), equation (2-29) becomes

$$c_2^2 - c_1^2 = -\frac{\gamma-1}{2}(u_1-u_2)\left[(u_1-u_2) \pm 2U\right] \tag{2-31}$$

From equation (2-27), we get

$$\rho_2 = \frac{\rho_1 U}{U \pm (u_1-u_2)} \tag{2-32}$$

Substituting (2-32) in (2-28) we obtain

$$p_1 - p_2 = \pm \rho_1 U (u_1-u_2) \tag{2-33}$$

Equation (2-33) can be written as

$$\frac{c_1^2 \rho_1}{\gamma} - \frac{c_2^2 \rho_2}{\gamma} = \pm \rho_1 U (u_1-u_2) \tag{2-34}$$

Eliminating ρ_2 from (2-34) with equation (2-32) and rearranging, we get

$$c_1^2 - \frac{U c_2^2}{U \pm (u_1-u_2)} = \pm \gamma U (u_1-u_2) \tag{2-35}$$

Elimination of c_2^2 from (2-31) with the help of equation (2-35), we have

$$u_2 = u_1 \pm \frac{2c_1}{\gamma+1}\left(\frac{U}{c_1} - \frac{c_1}{U}\right) \tag{2-36}$$

Substituting u_2 from equation (2-36) into equation (2-33), writing

$\rho_1 = \gamma \frac{p_1}{c_1^2}$, and then solving for U yields

$$U = c_1 \sqrt{\frac{\gamma+1}{2\gamma}\left(\frac{p_2}{p_1} - 1\right) + 1} \tag{2-37}$$

Substituting u_2 from equation (2-36) into equation (2-31) and solving for c_2 yields

$$c_2 = c_1 \sqrt{1 + \frac{2(\gamma-1)}{(\gamma+1)^2}\left[\gamma\left(\frac{U}{c_1}\right)^2 - \left(\frac{c_1}{U}\right)^2 - (\gamma-1)\right]} \tag{2-38}$$

Equations (2-36), (2-37) and (2-38) are the ones actually used in the calculations. For very strong shocks where $\frac{p_2}{p_1} >> 1$, equation (2-37) can sometimes be approximated by

$$U \approx c_1 \sqrt{\frac{\gamma+1}{2\gamma}\left(\frac{p_2}{p_1}\right)} \tag{2-39}$$

It is evident from equation (2-39) that $\frac{U}{c_1} >> 1$. Consequently equations (2-36) and (2-38) can be approximated by the following simple forms:

$$u_2 = u_1 \pm \frac{2U}{\gamma+1} \tag{2-40}$$

$$c_2 = \frac{\sqrt{2\gamma(\gamma-1)}}{\gamma+1} U \tag{2-41}$$

Strong shock equations, (2-39), (2-40) and (2-41) are used in the calculations of the blast waves where these relations are consistent with the similarity solution of the blast wave.

III SOLUTION OF THE PRESENT PROBLEM

1. Choice of the Basic Numerical Technique

There are two major basic numerical techniques in the application of the method of characteristics. One is the standard technique of integration along the two main characteristics, while the other follows the Hartree scheme, which involves fixed time intervals. These techniques were discussed and their applications were demonstrated in (23), (24) and (25), where it has been shown that both numerical schemes produce very accurate results when applied to the blast wave problem, provided the region with extremely high speed of sound is excluded. It is reasonable to assume that either of the two methods will yield accurate results when applied to the expansion of high pressure sphere.

In applying the standard technique, the points of intersection of two families of characteristics do not occur at equal intervals in either the space or time coordinates. When the spatial distribution of the flow variables at a later instant is required, we have to perform a two-dimensional interpolation, which is not always desirable.

The constant time technique overcomes the difficulty of uneven distribution of grid points by choosing grid points on predetermined constant time lines. This has the advantage that the required interpolation is always one dimensional.

The Hartree scheme gives results along particle paths in successive steps, therefore it is advantageous in dealing with present problem where an interface (contact surface) is involved. Difficulty may arise in applying the standard technique to solve problems, where shock formation is expected. Suppose the solution along characteristic $\overline{OA}$

and to the left of it (see Fig. 1) has been obtained without the prior knowledge of the formation of a shock at B which is the intersection of two characteristics of the same family. Let $\overline{BL}$ be the subsequent shock path; then the solution in the region $\overline{ABL}$ is wrong, since no account was taken of the shock to establish it. To obtain the solution in this region, the data required such as solutions at points 1, 2, 3 and 4 are generally destroyed in order to save storage space. This difficulty can be overcome either by keeping the points, at which the shock is most likely to occur, at greater time values than their neighboring points or by retaining large amounts of data, which might be useful for corrections due to the occurrence of the shock, in the memory. The former method causes complications in programming logic and the latter needs extra memory spaces. They are both undesirable in computer calculations.

The shortcomings of the Hartree scheme are generally believed to be that it is less accurate and more time consuming. Nevertheless, the results of the calculation for the plane blast wave by the standard technique and Hartree technique showed that the same accuracy was reached by both methods within comparable computer time. The main reason for this favorable result is because in applying the constant time method, the initial data points are on the same time line, therefore quadratic interpolation can easily be used in determining the flow properties at points other than the initial data points. As quadratic interpolations are generally more accurate than linear interpolations, this in turn improves the accuracy of the new point to be calculated. Consequently, in applying the Hartree technique, we are able to start with fewer initial data points in the beginning of calculation and still attain the same degree of accuracy. As a result, this compensates to the same extent the time required in carrying

out extra interpolations. It may also be attributed to the more even distribution of data points throughout the region of calculation when the Hartree scheme is used. By now it is evident that the Hartree technique is preferable for application to the present problem.

Although the basic numerical technique for the Hartree scheme of method of characteristics has been developed in reference (25), nevertheless, due to the complexity of the present problem, quite a few difficult points still need to be resolved. In this section, the method of handling the initial singularity, methods of initiation of the second shock, and some other problems pertaining to the solution of the present problem will be discussed.

2. Starting Singularity

Immediately after the release of the high pressure sphere, an outward traveling shock, which will be referred to later as the main shock to distinguish it from the second shock formed at a later time, propagates into the stagnant air; in addition, a contact surface which separates the gas and the air, and a centered rarefaction wave, are initiated from the boundary. (See Fig. 2) The existence of a second shock at the tail of the rarefaction has been discussed by many authors, i.e., Wecken (10), Whitham (8), Berry and Holt (19), etc. It is also known that the strength of such a shock is zero at the beginning and remains very weak in the early stage of the expansion. (See initiation of second shock.) Therefore, to avoid further complication of the already very intricate starting singularity, no second shock was introduced in the initial singularity. This introduces practically no error at all, since the error in not considering the

second shock is of third order, which is practically zero at this stage.

At $t = 0^+$, the time increment Δt approaches to zero and differences in characteristic equations between the plane and spherical cases vanish.

For a given high pressure sphere surrounded by atmospheric conditions all the flow properties are specified for points 1 and 2. What has to be established are the properties at points 3 and 4. Point 3, situated between the tail of the rarefaction wave and the contact surface represents the expanded gas on the left of the contact surface, while point 4 corresponds to the air engulfed by the outward propagating shock on the other side of the contact surface. Notice that across the contact surface, the pressure and velocity are continuous, i.e., $p_3 = p_4$ and $u_3 = u_4$. However, the speed of sound c_3 may be different from c_4. This depends on the initial conditions of the high pressure gas and that of the atmospheric air.

Flow properties at points 3 and 4 can be determined analytically by the shock relationships between points 1 and 4, the isentropic expansion relation between points 2 and 3, and the boundary conditions across the contact surface, $u_3 = u_4$ and $p_3 = p_4$.

For the centered rarefaction wave the flow is isentropic, and points 2 and 3 are on a I characteristic line. When the state characteristic equation (2-14) is simplified for the plane case ($\nu = 1$), we have

$$(du)_I = -\frac{1}{\rho c}(dp)_I \qquad (3-1)$$

For isentropic flow of polytropic gas with $\gamma = \gamma_2$ the following relationships hold

$$c^2 = \gamma_2 \frac{p}{\rho} \tag{3-2}$$

$$p\,\rho^{-\gamma_2} = \text{constant} = K_1 \tag{3-3}$$

With equations (3-2) and (3-3), we can write:

$$c^2 = K_1 \gamma_2 \rho^{\gamma_2 - 1} \tag{3-4}$$

Putting equation (3-4) in differential form, we obtain

$$2c\,dc = K_1 \gamma_2 (\gamma_2 - 1) \rho^{\gamma_2 - 2} d\rho \tag{3-5}$$

Dividing (3-5) by c^2, we get

$$2\frac{dc}{c} = (\gamma_2 - 1)\frac{d\rho}{\rho} \tag{3-6}$$

Differentiating (3-3) and rearranging yields

$$dp = \gamma_2 \frac{p}{\rho} d\rho = c^2 d\rho \tag{3-7}$$

Eliminating $d\rho$ from equations (3-7) and (3-5) we have the expression:

$$2c = (\gamma_2 - 1)\frac{dp}{\rho c} \tag{3-8}$$

Again by elimination of dp from equation (3-1) and (3-8), we finally get

$$(du)_I = -\frac{2}{\gamma_2 - 1}(dc)_I \tag{3-9}$$

Therefore $u_3 - u_2 = -\frac{2}{\gamma_2 - 1}(c_3 - c_2)$. With $u_2 = 0$

$$u_3 = -\frac{2}{\gamma_2 - 1}(c_3 - c_2)$$

This equation can be written as

$$\frac{u_3}{c_2} = \frac{2}{\gamma_2 - 1}\left(1 - \frac{c_3}{c_2}\right) \tag{3-10}$$

Introducing the isentropic relation between points 3 and 2

$$\frac{p_3}{p_2} = \left(\frac{c_3}{c_2}\right)^{\frac{2\gamma_2}{\gamma_2 - 1}}$$

equation (3-10) becomes

$$\frac{u_3}{c_2} = \frac{2}{\gamma_2 - 1}\left[1 - \left(\frac{p_3}{p_2}\right)^{\frac{\gamma_2 - 1}{2\gamma_2}}\right] \tag{3-11}$$

For the rightward traveling shock with $u_1 = 0$ and $\gamma = \gamma_1$, the corresponding shock equations (2-36) and (2-37) are

$$u_4 = \frac{2}{\gamma_1 + 1}\left(\frac{U_4}{c_1} - \frac{c_1}{U_4}\right) \tag{3-12}$$

and

$$U_4 = c_1 \sqrt{\frac{\gamma_1+1}{2\gamma_1}\left(\frac{p_4}{p_1}-1\right)+1} \tag{3-13}$$

Eliminating U_4 from equations (3-12) and (3-13), we obtain

$$\frac{u_4}{c_1} = \frac{\frac{p_4}{p_1}-1}{\gamma_1\sqrt{1+\frac{\gamma_1+1}{2\gamma_1}\left(\frac{p_4}{p_1}-1\right)}} \tag{3-14}$$

Since $u_4 = u_3$ and $p_4 = p_3$, equation (3-11) is equivalent to

$$\frac{u_4}{c_2} = \frac{2}{\gamma_2-1}\left[1-\left(\frac{p_4}{p_2}\right)^{\frac{\gamma_2-1}{2\gamma_2}}\right] = \frac{2}{\gamma_2-1}\left[1-\left(\frac{p_1}{p_2}\right)^{\frac{\gamma_2-1}{2\gamma_2}}\left(\frac{p_4}{p_1}\right)^{\frac{\gamma_2-1}{2\gamma_2}}\right] \tag{3-15}$$

Equating the expressions for u_4 in equations (3-14) and (3-15) and solving for $\frac{p_1}{p_2}$, we get:

$$\frac{p_1}{p_2} = \frac{p_1}{p_4}\left[1-\frac{\gamma_2-1}{2\gamma_1}\left(\frac{c_1}{c_3}\right)\frac{\frac{p_4}{p_1}-1}{\sqrt{1+\frac{\gamma_1+1}{2\gamma_1}\left(\frac{p_4}{p_1}-1\right)}}\right]^{\frac{2\gamma_2}{\gamma_2-1}} \tag{3-16}$$

Here in equation (3-16), p_4 is the only unknown. Once the initial conditions of the gas as well as that of the atmospheric air are known, p_4 can be evaluated.

The Newton-Raphson iterative process was used in the calculation of p_4 and no difficulties have been encountered. After p_4 is determined, the remaining unknowns can be obtained in the following fashion: the shock velocity can be calculated from equation (3-13),

then u_4 and c_4 can be evaluated from equations (3-12) and (2-38),* respectively. Since $p_4 = p_3$ and $u_4 = u_3$, the only unknown left is c_3 which can easily be obtained from equation (3-10). Now everything has been determined for $x = x_o$ and $t = 0^+$.

Again, referring to Fig. 2, at time $t = t_2 = \Delta t$ (a small time interval) the physical locations of points 8, N, 5 and 7 as well as the flow properties between 8 and 7 are to be determined.

For a very small time interval, Δt, the flow properties in the regions $\overline{N05}$ and $\overline{607}$ vary very little. Therefore, in changing the differential equations into corresponding finite difference equations and interpolating properties between points can be made without incurring much inaccuracy. However, this is not the case for region $\overline{80N}$, the centered rarefaction wave region, where flow properties, even though continuous, vary very rapidly with respect to both x and t, no matter how small Δt is. To overcome this difficulty, the centered rarefaction wave region was divided into many small segments separated by the II characteristics issuing from point 0.

At point 0, the pressure difference between neighboring II characteristics are chosen to be equal. It is known that flow properties change gradually along each II characteristic. Therefore the variation of flow properties within each segment will be small. Hence it is permissible to obtain the solutions for points from 8 to N successively with finite difference equations along characteristic directions.

---

* Replacing subscript 2 with 4.

Since the head of the rarefaction wave propagates with a velocity u - c, where u = 0 and c = c_2 = constant for the undisturbed gas, therefore, $\overline{08}$ traces a straight line with slope $\left(\frac{dx}{dt}\right)_{II} = -c_2$. Knowing the location of point 8 and all the flow properties along $\overline{28}$, the solution for point 9 can be established.

Let 9' be a point on $\overline{09}$ near point 0, then the pressure at point 9' $p_{9'} = p_2 + \frac{p_3 - p_2}{M}$, where M is the total number of segments chosen in the rarefaction wave region. The particle velocity u_9, and speed of sound c_9, can be calculated from equations (2-23) and (3-9).

$$c_{9'} = c_2 \left(\frac{p_{9'}}{p_2}\right)^{\frac{\gamma_2 - 1}{2\gamma_2}}$$

and

$$u_{9'} = u_2 - \frac{2}{\gamma_2 - 1}\left(c_{9'} - c_2\right)$$

where $u_2 = 0$

Knowing the location of point 8, all the flow properties along $\overline{28}$, and the initial slope of the II characteristic line at 9', the solution for point 9 can be established with the help of the six finite-difference equations along the three characteristic directions. This is accomplished by iterative process similar to the one used for the interior points, (see Ref. (25)) with the only exception that the initial data are not located at a constant time line.

Essentially the same procedure can be used to obtain solution for points 10 to N successively. Here the distribution of flow properties along each of the II characteristics is assumed to be linear.

The solutions for points 5, 6 and 7 are interrelated. They have to be solved simultaneously through a rather complicated system of algebraic finite-difference equations. They are (refer to Fig. 2) finite-difference equations derived from physical characteristic equations,

Along I_g $$\frac{x_5 - x_A}{\Delta t - t_A} = \frac{u_A + u_5}{2} + \frac{c_A + c_5}{2} \qquad (3\text{-}17)$$

Along III_g $$\frac{x_5 - x_o}{\Delta t} = \frac{u_3 + u_5}{2} \qquad (3\text{-}18)$$

Along I_a $$\frac{x_7 - x_c}{\Delta t - t_c} = \frac{u_c + u_7}{2} + \frac{c_c + c_7}{2} \qquad (3\text{-}19)$$

Along II_a $$\frac{x_6 - x_B}{\Delta t - t_B} = \frac{u_B + u_6}{2} - \frac{c_B + c_6}{2} \qquad (3\text{-}20)$$

Along III_a $$\frac{x_6 - x_o}{\Delta t} = \frac{u_4 + u_6}{2}$$

(This equation is identical with equation (3-18) because $x_6 = x_5$, $u_4 = u_3$ and $u_6 = u_5$)

And finite-difference equations derived from state characteristic equations:

Along I_g $$u_5 - u_A = -\frac{c_5 + c_A}{\gamma_2 (\rho_5 + \rho_A)} (\rho_5 - \rho_A) - \frac{(u_5 + u_A)(c_5 + c_A)}{x_5 + x_A} (\Delta t - t_A) \qquad (3\text{-}21)$$

Along III_g $$\frac{p_5}{p_3} = \left(\frac{c_5}{c_3}\right)^{\frac{2\gamma_2}{\gamma_2-1}} \tag{3-22}$$

Along I_a $$u_7 - u_c = -\frac{c_7+c_c}{\gamma_1(p_7+p_c)}(p_7-p_c) - \frac{(u_7+u_c)(c_7+c_c)}{x_7+x_c}(\Delta t - t_c) \tag{3-23}$$

Along II_a $$u_6 - u_B = \frac{c_6+c_B}{\gamma_1(p_6+p_B)}(p_6-p_B) + \frac{(u_6+u_B)(c_6+c_B)}{x_6+x_B}(\Delta t - t_B) \tag{3-24}$$

Along III_a $$\frac{p_6}{p_4} = \left(\frac{c_6}{c_4}\right)^{\frac{2\gamma_1}{\gamma_1-1}} \tag{3-25}$$

The shock relations

$$U_7 = c_1\sqrt{\frac{\gamma_1+1}{2\gamma_1}\left(\frac{p_7}{p_1}-1\right)+1} \tag{3-26}$$

$$u_7 = \frac{2c_1}{\gamma_1+1}\left(\frac{U_7}{c_1} - \frac{c_1}{U_7}\right) \tag{3-27}$$

$$c_7 = c_1\left\{1 + \frac{2(\gamma_1-1)}{(\gamma_1+1)^2}\left[\gamma_1\left(\frac{U_7}{c_1}\right)^2 - \left(\frac{c_1}{U_7}\right)^2 - (\gamma_1-1)\right]\right\}^{\frac{1}{2}} \tag{3-28}$$

By the definition of velocity of the shock, we can write

$$\left(\frac{dx}{dt}\right)_{shock} = U = \frac{U_7+U_4}{2} = \frac{x_7-x_0}{\Delta t} \tag{3-29}$$

Assume that Δt is small enough such that within the region under consideration, the tail of the rarefaction wave, the contact surface and the shock front can be approximated by straight lines. And furthermore we assume that the flow properties are linearly distributed along these lines. Then we may write

$$\frac{x_N - x_0}{\Delta t} = \frac{x_A - x_0}{t_A} \tag{3-30}$$

$$\frac{x_6 - x_0}{\Delta t} = \frac{x_c - x_0}{t_c} \tag{3-31}$$

$$\frac{x_7 - x_0}{\Delta t} = \frac{x_B - x_0}{t_B} \tag{3-32}$$

and nine linear interpolation equations for flow properties at points A, B and C. Since solutions at points 3 and 4 are known from the previous calculations, suppose Δt has been preselected (to be discussed later), then the total number of variables involved in the above equations are 28, namely: x_5, u_5, c_5, p_5, x_6, u_6, c_6, p_6, x_7, u_7, c_7, p_7, U_7, x_A, t_A, u_A, c_A, p_A, x_B, t_B, u_B, c_B, p_B, x_c, t_c, u_c, c_c and p_c. Because 5 and 6 are points on two sides of the contact surface, $u_5 = u_6$, $p_5 = p_6$ and $x_5 = x_6$, this reduces the total number of unknowns to 25. Equations (3-17) to (3-32) comprise 16 equations. Adding nine interpolation equations, we have exactly 25 equations to solve for the 25

unknowns. The solution of the above system of equations was accomplished by iterative processes.

The accuracy of the numerical scheme was checked by applying it to the numerical example given by McFadden (18) and the results were compared.

McFadden took the case of the expansion of a high pressure gas sphere, initially at rest, into surrounding air. Both the high pressure gas and the ambient air are assumed to be diatomic gases with $\gamma = 1.4$. The initial pressure ratio of the gas to that of the surrounding air is 12.8173 and the density ratio is 3.9560. Comparable results at a time when the head of the rarefaction wave traveled a distance of 5% of the initial radius of the gas sphere are as follows.

	McFadden's series solution	Results by method of characteristics
x_s*	1.055 †	1.055
x_i	1.035 †	1.035
x_t	0.992 †	0.992
$\frac{p_s}{p_1}$	4.33 **	4.333
$\frac{p_i}{p_1}$	4.29 **	4.298
$\frac{p_t}{p_1}$	4.24 **	4.236

* x denotes the physical position and the subscripts s, i, and t are used for the shock front, the contact surface and the tail of the rarefaction wave, respectively.

† values calculated according to McFadden's solutions.

** values presented by McFadden.

Considering the fact that these results by method of characteristics were obtained through a single time step, it is gratifying to see such a good agreement with McFadden's series solution. In the actual calculation of the high pressure sphere, smaller time steps (approximately half) are employed. Therefore, the claims for accuracy of this numerical procedure are warranted.

3. Second Shock

After the release of a high pressure sphere, in addition to the main shock propagating into the atmosphere, there exists another shock wave, which is usually referred to as the second shock, formed at the tail of the rarefaction wave traveling into the expanding gas. The existence of the second shock was first predicted by Wecken (10) on the basis of extensive numerical calculations of a spherical blast from certain explosions. Berry and Holt (19) analyzed the initial disturbance of the spherical blast from certain explosions by series expansions and showed that the singular characteristic initially in the direction of the tail of the rarefaction wave developed into a shock wave. The same phenomenon is found to occur for the expansion of a uniform high pressure sphere as a result of the formation of a compression wave behind the tail of the rarefaction wave. If a very small left traveling discontinuity is introduced, it grows steadily into a finite shock.

The second shock, though growing with time, remains very weak until the time when the head of the rarefaction wave reaches the center

of the sphere, then it starts to grow in strength rapidly. The strength of a shock is defined as the ratio of the difference in pressure across the shock to the pressure in front of the shock. Since there is no second shock at $t = 0$, and the initial rate of growth is slow, therefore exactly where or how large an initial shock discontinuity to be introduced in the beginning is of little influence in the general results, as long as it is inserted before the head of the rarefaction wave reaches the center and the magnitude of the discontinuity is very small. This fact can be observed in Fig. 3 and Fig. 4, where curves showing position and the strength of second shock vs time are plotted for shocks initiated at different times and with different initial discontinuities. These curves also can serve the purpose of showing the general behavior of the second shock. It is called a left traveling shock because it propagates toward the left with respect to the gas particles in front of it. Depending on the values of the particle velocity u and the shock velocity U, the absolute velocity of the shock front may move toward either left or right. However, as the shock grows in strength, it will eventually acquire an absolute velocity toward the center of the sphere.

The general procedure in the initiation of the second shock is described as follows:

Suppose a second shock is to be initiated at the time $t = t_2$ (see Fig. 5), then the calculation in the rarefaction wave region will end at point 8, which is on the II characteristic immediately adjacent to the left of the tail of the rarefaction wave.

The shock at point 7 is initiated by inserting a shock discontinuity of negligible strength at point 2 on the initial time line. Let $\frac{p_3 - p_2}{p_2} = \epsilon \ll 1$, then u_3, c_3 and U_3 can be calculated from the shock relations

$$U_3 = c_2 \sqrt{\frac{\gamma_2 + 1}{2\gamma_2}\left(\frac{p_3}{p_2} - 1\right) + 1}$$

$$c_3 = c_2 \sqrt{1 + \frac{2(\gamma_2 - 1)}{(\gamma_2 + 1)^2}\left[\gamma_2\left(\frac{U_3}{c_2}\right)^2 - \left(\frac{c_2}{U_3}\right)^2 - (\gamma_2 - 1)\right]}$$

$$u_3 = u_2 - \frac{2c_2}{\gamma_2 + 1}\left(\frac{U_3}{c_2} - \frac{c_2}{U_3}\right)$$

Now everything is known for points 8, 1, 2, 3, 4 and 5. Write the finite-difference equation for physical and state characteristic equations.

Along I_1-characteristic

$$\frac{x_6 - x_A}{t_2 - t_A} = \frac{u_A + u_6}{2} + \frac{c_A + c_6}{2} \tag{3-33}$$

$$u_6 - u_A = -\frac{c_6 + c_A}{\gamma_2(p_6 + p_A)}(p_6 - p_A) - \frac{(u_6 + u_A)(c_6 + c_A)}{(x_6 + x_A)}(t_2 - t_A) \tag{3-34}$$

Along III_1-characteristic

$$\frac{x_6 - x_D}{t_2 - t_D} = \frac{u_D + u_6}{2} \tag{3-35}$$

$$\frac{p_6}{p_D} = \left(\frac{c_6}{c_D}\right)^{\frac{2\gamma_2}{\gamma_2 - 1}} \tag{3-36}$$

Along II_1-characteristic

$$\frac{x_6 - x_B}{\Delta t} = \frac{u_B + u_6}{2} - \frac{c_B + c_6}{2} \tag{3-37}$$

$$u_6 - u_B = \frac{c_6 + c_B}{\gamma_2 (p_6 + p_B)} (p_6 - p_B) + \frac{(u_6 + u_B)(c_6 + c_B)}{(x_6 + x_B)} \Delta t \tag{3-38}$$

Along II_2-characteristic

$$\frac{x_6 - x_c}{\Delta t} = \frac{u_7 + u_c}{2} - \frac{c_7 + c_c}{2} \tag{3-39}$$

$$u_7 - u_c = \frac{c_7 + c_c}{\gamma_2 (p_7 + p_c)} (p_7 - p_c) + \frac{(u_7 + u_c)(c_7 + c_c)}{(x_7 + x_c)} \Delta t \tag{3-40}$$

Across the shock we can write:

$$U_7 = c_6 \sqrt{\frac{\gamma_2 + 1}{2\gamma_2} \left(\frac{p_7}{p_6} - 1 \right) + 1} \tag{3-41}$$

$$u_7 = u_6 - \frac{2 c_6}{\gamma_2 + 1} \left(\frac{U_7}{c_6} - \frac{c_6}{U_7} \right) \tag{3-42}$$

$$c_7 = c_6 \sqrt{1 + \frac{2(\gamma_2 - 1)}{(\gamma_2 + 1)^2} \left[\gamma_2 \left(\frac{U_7}{c_6} \right)^2 - \left(\frac{c_6}{U_7} \right)^2 - (\gamma_2 - 1) \right]} \tag{3-43}$$

From the definition of shock velocity

$$\frac{x_6 - x_2}{\Delta t} = \frac{u_2 - U_3 + u_6 - U_7}{2} \tag{3-44}$$

Assuming the II_1 characteristic $\overline{18}$ is a straight line, then two more equations can be written:

$$\frac{\Delta t}{x_8 - x_1} = \frac{t_2 - t_A}{x_8 - x_A} \tag{3-45}$$

$$\frac{\Delta t}{x_8 - x_1} = \frac{t_2 - t_D}{x_8 - x_D} \tag{3-46}$$

By assuming the flow properties are linear along $\overline{18}$ and $\overline{12}$ yields nine equations for linear interpolation of properties at A, D and B. Since the flow properties varying rapidly between points 3, 4 and 5, three quadratic interpolation formulas were used in determining u_C, c_C, and p_C. Adding the 12 equations from interpolating the flow properties to the 14 equations (3-33) to (3-46), makes a total of 26 equations. There are exactly 26 unknowns, namely: x_6, u_6, c_6, p_6, U_7, u_7, c_7, p_7, x_A, t_A, u_A, c_A, p_A, x_D, t_D, u_D, c_D, p_D, x_B, u_B, c_B, p_B, x_C, u_C, c_C, and p_C. The approximate solution of this system of equations can be arrived at through an iterative process without difficulty.

4. Contact Surface

One of the advantages of applying the Hartree scheme in the calculation of the present problem can be appreciated from the easiness in treating the contact surface. Since the contact surface is formed by particle paths, essentially the same numerical scheme as for the interior points can be used with the only difference being that the isentropic

relations along particle paths yield two equations rather than one equation in the case of an interior point. This is because across a contact surface pressure and particle velocity are continuous but the speeds of sound usually are different. Finite-difference equations along characteristic directions are similar to those of the interior points which are shown in reference (25). In the solution of these equations almost the same iterative procedure for the interior points can be employed.

5. Choice of Time Step

The choice of the magnitude of the first time step Δt_1 is arbitrary except for reasons of accuracy and computational effort. This time step is usually kept in a range that in such a time interval the head of the rarefaction travels a distance approximately equal to 3% of the initial radius of the high pressure sphere.

In the subsequent calculations, the Courant condition $\Delta t < \frac{\Delta x}{c}$, which was discussed in reference (25), is observed. However, before the head of the rarefaction reaches the center, the choice of time steps are further limited to be not greater than Δt_1, the very first time interval selected. Within the domain of these limitations we have always chosen the largest time steps allowable.

In determining the time step for a new time line, it is necessary to scan through all the neighboring data points on the initial constant time line and select the largest time interval permissible. A data point distribution, along a constant time line, which makes every local

maximum allowable Δt the same would be most desirable for the sake of computing effort. However, generally this is not possible. Nevertheless, with this in mind, we occasionally rearranged the distribution of initial data points in the course of the computer calculation.

IV RESULTS

Due to the complex nature of the flow field, the calculation is divided into three stages, as shown schematically in Fig. 6. The first stage of calculation starts from $t = 0$ and ends at the time when the head of the rarefaction reaches the center of the sphere. The second stage of calculation terminates just before the inward shock reaches the center of the sphere. The third stage includes a triangular region bounded by the constant time line $\overline{AB}$, the shock front $\overline{BD}$, and a line $\overline{AD}$. Point A is placed some distance away from the center. The slope of $\overline{AD}$ is chosen to be smaller than that of the local I characteristic, (because the condition $\Delta t < \frac{\Delta x}{c}$) thus the reflected second shock does not affect the region to the right of line $\overline{AD}$.

In order to make the results more general, the dependent variables u, c, p and the independent variables x and t were non-dimensionalized with appropriate parameters of the atmospheric air and the initial total energy released in the expanding sphere. The non-dimensional variables include:

pressure $$\pi = \frac{p}{p_1}$$

particle velocity $$\beta = \frac{u}{c_1}$$

speed of sound $\Theta = \frac{c}{c_1}$

density $\eta = \frac{\rho}{\rho_1}$

radius $\lambda = \frac{x}{\xi}$

1. General Features

The general behavior of the expansion of a high pressure sphere can best be shown by a numerical example. Results of the expansion of a high pressure sphere initially with pressure ratio $\pi_0 = 100$, density ratio $\eta_0 = 1.16$, and $\gamma_2 = 1.4$ as calculated by the Hartree scheme, are shown in Fig. 7 to Fig. 12.

Fig. 7 shows the propagation of the main shock followed by the contact surface; both travel outward with decreasing speeds. A second shock appears at a later time, even though it travels to the left relative to the gas, for a moment it is moving with an absolute velocity toward the right. However, as the second shock gains strength with time, it soon acquires an inward moving speed and then races toward the center at an accelerated pace.

The decay of the peak pressure, $\pi_s = \frac{p_s}{p_1}$, where p_s is the pressure immediately behind the main shock, is shown in Fig. 8. The rate of decay decreases as the main shock moving to a larger radius. Pressure profiles are shown in Fig. 9 and Fig. 10. The first curve ($\tau = 0$) in Fig. 9 is the initial pressure distribution, and the second curve

(τ = 0.0026) shows the pressure profile shortly after the release. The rarefaction wave moves toward the center of the sphere and reaches there at τ = 0.023. By that time the second shock is already formed. Notice the lowest pressure occurs at the tail of the rarefaction wave. To its right pressure increases with λ, the non-dimensional radius, and reaches a peak at the shock front. At the contact surface, which is marked by a bar, pressure is continuous, but its derivative with respect to λ is not. For clarity, curves shown in Fig. 10 are drawn with a different scale from that used in Fig. 9. If this is unnoticed the general appearance may be deceiving. At τ = 0.030 the second shock already gained considerable strength, and attained its extreme right position. This rapid increase in shock strength is primarily due to the diminishing of pressure in front of the second shock. After the main shock propagates quite a distance, the pressure gradient behind it gradually decreases. This can be seen by comparing the three curves on the extreme right.

Fig. 11 shows the profiles of the particle velocity at various time instants. Particles, gaining speed through the expansion wave, reach their peak velocity at the tail of the rarefaction wave. It is interesting to see that at τ = 0.045 the particle velocity behind the second shock becomes negative, which means gas particles are pushed back toward the center. This negative velocity reaches very high value just before the second shock implodes on the center of the sphere.

The profiles of the speed of sound $\theta = \frac{c}{c_1}$, are presented in Fig. 12. Since for a polytropic gas, temperatures is proportional to square of

the velocity of sound, therefore these curves can be interpreted as the temperature profile with square root of temperature ratio, $\frac{T}{T_i}$, as ordinate. Initially the high pressure gas is at a much higher temperature than that of the outside air. Immediately after the release, gas temperature reduces through expansion and in the mean-time air temperature rises after experiencing a shock. However, the difference in temperature remains quite large across the contact surface which separates them. It is shown that there is a big jump in speed of sound from the right to the left across the contact surface. The speed of sound at the center becomes progressively lower as a result of expansion, but the implosion of the second shock will raise it again.

In an attempt to investigate whether the distribution of the flow properties of the expanding high pressure sphere at late times approaches that of Sedov's blast wave solution, the distribution of the three flow properties were once again plotted in a somewhat different fashion. Fig. 13 shows the ratio of local pressure to the corresponding peak pressure against the ratio of local radius to the corresponding radius of the main shock front, for several late times. The solid curve labeled as Sedov's blast wave solution was based on the numerical values given by Sedov (2). Similar curves for particle velocity and speed of sound were presented in Figures 14 and 15. It is seen that the pressure distribution adjacent to the main shock front for the expanding sphere approaches that of the Sedov's blast wave solution as time

elapses. However this conclusion cannot be applied to the other two flow properties, particle velocity and speed of sound. In fact as a whole the flow field resulted from the expansion of a high pressure sphere is quite different from that of Sedov's blast wave solution. Nevertheless the destructive effect of a blast wave usually is determined by the peak pressure of the blast. As will be shown later in the section on late-stage equivalence, the peak pressure of an expanding high pressure sphere can be approximated by the corresponding Sedov's solution with equal total initial energy in a region when the main shock has propagated some distance, and the peak pressure still above 10 atm. Therefore, for a rough estimation of the damaging effect resulting from the shock pressure of the expansion of a high pressure sphere, the corresponding Sedov's blast wave solution, equal energy, can be used.

Some numerical results of the expansion of high pressure spheres were reported previously by Brode (26). Those results were presented in rather sketchy curves with ill-defined boundaries. Therefore, it is impossible to make a precise assessment of their accuracy. However, judging from our calculations of one of Brode's examples, his results are in considerable error, even in the region corresponding to our first stage of calculation. The error in peak pressure is estimated to be of the order of 10%. Even larger errors, more than 20%, in pressure occurred in the rarefaction wave region. Moreover, the pressure profile Brode identified as second shock was so widely spread that it could hardly be called a shock. Nevertheless, despite all these discrepancies,

qualitatively Brode's results are in general agreement with our calculations.

2. Late-Stage Equivalence

A. Late-stage equivalence in hypervelocity impact.

Before we discuss the principle of late-stage equivalence in expanding high pressure spheres it seems appropriate to review some related background about the general concept of late-stage equivalence. The principle of late-stage equivalence was first proposed by Walsh et al (27) in studying effects of hypervelocity impact. It stipulates that projectiles of different mass and velocity striking a target will give rise to target flows very nearly identical at late times, provided the product of mass and the velocity raised to the α power ($M_0 V_0^{\alpha}$) is the same for all projectiles. This principle is assumed to be applicable within the hydrodynamic phase of the hypervelocity impact where the interaction is governed by equations of fluid dynamics prior to the onset of material strength effects. If two impact flows during the hydrodynamic phase of the interaction are equivalent, then the strength-dependent phase of the motions will also be equivalent. Therefore, the property of late-stage equivalence enables one to extrapolate the existing experimental results from impacts at comparatively low velocities attained in controlled experiments to the meteoric velocity which is not accessible to laboratory experiments.

For one-dimensional impacts of materials with ideal gas equation of state, Walsh et al (27) showed that by assuming impacts are late-

stage equivalent on the basis of $M_o V_o^{\alpha}$ rather than dependent on M_o and V_o individually led to the results that the flow is of self-similar type. The analytical similarity solution and a solution by finite-difference calculation (SPUTTER code) of an ideal-gas impact, with $\gamma = 1.4$ were found to be in good agreement at late times on the basis of equal $M_o V_o^{1.5}$. Recent work by Chou and Burns (28) reported extensive calculations for the same problem employing the method of characteristics demonstrated also that the shock fronts produced by different one-dimensional impacts approach each other in position and in strength at late times provided $M_o V_o^{1.5}$ is constant.

In the case of axisymmetric impact of ideal-gas the problem is fully characterized by given values of γ, the initial density ρ_o, the characteristic length of the projectile L_o, and the impact velocity v_o. From dimensional considerations, the solution must be functions of three non-dimensional variables, $\frac{r}{L_o}$, $\frac{z}{L_o}$ and $\frac{t V_o}{L_o}$, where r and z are cylindrical coordinates with origin at the center of the initial surface of impact. The assumption of late-stage equivalence on the basis of $M_o V_o^{\alpha}$ or $L_o V^{\frac{\alpha}{3}}$ is to require that the solution not contain L_o, V_o as individual parameters. The solution must approach at late time a flow expressible in the form:

$$\rho = \rho_o \, g_1\left(\frac{R^{\alpha'+1}}{\tau^{\alpha'}}, \frac{Z^{\alpha'+1}}{\tau^{\alpha'}}, \gamma\right)$$

$$P = \rho_0 V_0^2 g_2\left(\frac{R^{\alpha'+1}}{\tau^{\alpha'}}, \frac{Z^{\alpha'+1}}{\tau^{\alpha'}}, \gamma\right)$$

$$u = V_0 Z^{-\frac{1}{\alpha'}} g_3\left(\frac{R^{\alpha'+1}}{\tau^{\alpha'}}, \frac{Z^{\alpha'+1}}{\tau^{\alpha'}}, \gamma\right)$$

$$v = V_0 Z^{-\frac{1}{\alpha'}} g_4\left(\frac{R^{\alpha'+1}}{\tau^{\alpha'}}, \frac{Z^{\alpha'+1}}{\tau^{\alpha'}}, \gamma\right)$$

where $\tau = \frac{t V_0}{L_0}$, $R = \frac{r}{L_0}$, $Z = \frac{z}{L_0}$ and $\alpha' = \frac{\alpha}{3}$. This represents a similarity solution; i.e., the number of independent variables is reduced to two instead of the original three. The similarity solution apparently still cannot be solved analytically without additional approximations. However, it is possible from the form of the solution to determine the relation which must exist between the shock decay rate and α', shock pressure decays as $Z^{-\frac{2}{\alpha'}}$, and between the rate of increase of total positive axial and total positive radial momenta and α'. These integrated momenta increase as $t^{\frac{(3\alpha'-1)}{\alpha'+1}}$. This is because the distances increase as $t^{\frac{\alpha'}{\alpha'+1}}$, mass engulfed therefore increases as $t^{\frac{3\alpha'}{\alpha'+1}}$, and velocities decrease as $t^{-\frac{1}{\alpha'+1}}$, so that the momentum within corresponding elements of volume varies as $t^{\frac{3\alpha'-1}{\alpha'+1}}$. These results can be compared with the computed solution determined without

assuming late-stage equivalence. Walsh (27) calculated a problem of right circular cylinder of unit aspect ratio impacting a semi-infinite target using the Eulerian code, and found that the calculated solution agrees at late times with the similarity solution. The value of α' determined from the shock decay rate and the increase of momenta is $\alpha' = .59$ which corresponds to $\alpha = 1.77$. These results are for $\gamma = 1.5$.

For solid-solid impact, Riney (29) proposed a visco-plastic model which bridges the transition from the early hydrodynamic phase to the later stages when strain-rate and strength effects become important. Calculations for a cylindrical projectile impacting a thick target of like material at various velocities were carried out to the point where strain-rate and strength effects can no longer be neglected. Upon comparing the flow field resulting from impacts of different velocities Riney found that the flow fields are essentially equivalent except for the initial stage of the cratering process if the geometrically similar projectiles are chosen to have the same kinetic energy, $M_o V_o^2$, at impact.

In short, the concept of late-stage equivalence of hypervelocity impact on the basis of $M_o V_o^{\alpha}$ is established on numerical evidence rather than on theoretical grounds. However, the most important general conclusion from one-dimensional impact, the axisymmetric ideal gas impact and solid-solid impacts is that impacts are equivalent on a basis intermediate between equal projectile momentum and equal projectile energy.

B. Late-stage equivalence in expanding high pressure spheres

In view of the evidence of the late-stage equivalence in hypervelocity impact, it leads us to the investigation of similar equivalence in expansion of high pressure spheres. Based on the numerical results of the present calculation, late-stage equivalence is found to exist for the expansion of high pressure spheres with various initial conditions, provided the initial energy released, $E_o = \frac{4\pi}{3}\frac{(p_o - p_1)}{(\gamma-1)}x_o^3$, in each of the spheres is held constant. Late-stage equivalence is assumed to exist if the peak pressure distribution for different expanding spheres are the same at late times. This is demonstrated by Fig. 16 where peak pressure vs. radius curves of expanding spheres with equal initial energy E_o but different initial radius, pressure and density are shown in logarithmic scales. The purpose of choosing logarithmic scales is to cover the extremely wide range of peak pressures, from $\pi_o = 2000$ to $\pi_o = 2$, in a single plot. Accompanying these curves the corresponding point source solution is also included in the plot. The point source solution represents the extreme case of a high pressure sphere of zero radius.

In the high pressure region, the peak pressure distribution of the point source solution can be derived from equations given by Sedov (2).

$$p_s = \frac{8E}{(\nu+2)^2(\gamma+1)}\frac{1}{x_s^\nu} = \frac{8E}{25(\gamma+1)}\frac{1}{x_s^3}$$

where p_s is the peak pressure, x_s is the position of the shock front and E is a constant proportional to E_o, the total energy released initially. According to the point charge formulation the total energy of the disturbed gas remains constant. Therefore, we have

$$E_o = \int_o^{x_s} \frac{\rho u^2}{2} 4\pi x^2 dx + \int_o^{x_s} \frac{p}{\gamma-1} 4\pi x^2 dx$$

The first term is the kinetic energy and the second term is the internal energy. Introducing non-dimensional quantities, we can write

$$E_o = \left\{ 2\pi \int_o^1 R V^2 \lambda^2 d\lambda + \frac{4\pi}{\gamma-1} \int_o^1 P \lambda^4 d\lambda \right\} E$$

where

$$R = \frac{\gamma+1}{\gamma-1} \frac{\rho}{\rho_s}$$

$$V = \frac{4}{5(\gamma+1)\lambda} \frac{u}{u_s}$$

$$P = \frac{8\gamma}{25(\gamma+1)\lambda^2} \frac{p}{p_s}$$

$$\lambda = \frac{x}{x_s}$$

It can be shown that the sum of the integrals in the square bracket is a function of γ only and for $\gamma = 1.4$, $E = 1.175E_o$. Since ξ is defined as $\sqrt[3]{\frac{E_o}{p_1}}$, let λ_s be the non-dimensional radius of the shock front $\frac{x_s}{\xi}$, then the relation between peak pressure and position can be reduced to

the simple form,

$$\Pi_s = \frac{p_s}{p_1} = 0.1567\, \lambda_s^{-3}$$

This is shown by the straight line portion of the modified point source solution in Fig. 13. It is called "modified point source" because when the peak pressure ratio is less than 100, numerically calculated results are continued from the point source solution.

For peak pressure Π_s below 100, the point source solution is modified by taking into consideration the ambient pressure p_1. This is accomplished by carrying out a computation similar to the calculation of similarity solution of blast wave by standard method of characteristics, except this time exact shock relations, equations (2-36) to (2-38), instead of the strong shock approximations, equations (2-39) to (2-41), are utilized in the calculation. Numerical results obtained are found to be in extremely good agreement with those of Goldstein's (3). The graphical representation of the modified peak pressure distribution appears in Fig. 16 as a curved line with a positive radius of curvature.

To keep the initial energy released constant, spheres with higher initial pressure are associated with smaller radii. It is seen that the peak pressure curve of a sphere with higher initial pressure decays faster and coalesces with those started at lower initial pressure and they all finally approach the modified point source solution. Notice in every case, immediately after the release, the peak pressure is much lower than the corresponding peak pressure of the point source solution,

but it decays at a slower rate and exceeds the modified point source solution before they finally coalesce.

If in addition we require the initial energy released to be constant, the total mass, $\frac{4\pi}{3}\rho_0 x_0^3$, is also kept constant, the late-stage equivalence exists not only for peak pressure of the main shock, but also for the positions for both the main shock and the second shock in the physical plane (λ-τ plane). This is revealed in Fig. 17 where the main shock front, contact surface and the second shock are presented for high pressure spheres with initial pressure ranging from $\pi_0 = 50$ to $\pi_0 = 500$. The late-stage equivalence in peak pressure can be seen in Fig. 18. This time, peak pressure curves are plotted in linear scales. Perhaps a presentation like this can be better appreciated. Once again, the four curves, for $\pi_0 = 500$, $\pi_0 = 200$, $\pi_0 = 100$ and $\pi_0 = 50$ converge together and approach the modified point source solution at late times.

V CONCLUSION

The Hartree scheme was successfully applied to the solution of the flow field of the expansion of high pressure spheres. A special technique designed to handle the starting singularity was found to be accurate. Results obtained by this method for the initial behavior of the spherical expansion agree very well with those calculated by McFadden's analytical solution.

The formation of a second shock from the previously continuous flow field was found to exist at the tail of the left traveling rarefaction wave. The strength of the second shock remains rather small before the head of the rarefaction wave reaches the center of the sphere, then it grows rapidly to very high strength. The path of the second shock in the physical plane is accurately defined and some interesting features are revealed.

The numerical results of a typical example of the expansion of a high pressure sphere were presented in graphs showing the propagation of the main shock, the development of the second shock and the propagation of the contact surface which separates the two fluids. The boundaries of these discontinuity surfaces were accurately revealed. Profiles of pressure, particle velocity and speed of sound at different times after the release were also depicted.

Based on numerous calculations, it is shown that "late-stage equivalence" exists in the expansion of high pressure spheres into the atmosphere, provided the initial total energy in each of the spheres is

kept constant. If the initial condition is further limited to equal masses, then the late-stage equivalence exists not only for peak pressure of the main shock but also for the position of both the main and the second shock in the x-t plane.

The method developed in this report can be extended to solve problems for perfect fluids with equations of state other than that of the polytropic gas. It may also be extended to radially symmetric problems with non-uniform initial properties and non-zero initial particle velocities.

REFERENCES

1. Taylor, G.I., "The Formation of a Blast Wave by a Very Intense Explosion, I, Theoretical Discussion," Proc. Roy. Soc. (London) A201, pp. 159-174, (1950).

2. Sedov, S. I., "Similarity and Dimensional Methods in Mechanics," Academic Press, New York, Chapter IV, pp. 146, (1959).

3. Goldstine, H. H., and Von Neumann, J., "Blast Wave Calculation," Commu. Pure and Applied Math., (1955).

4. Brode, H. L., "Numerical Solutions of Spherical Blast Waves," Jl. Applied Phys., (1955).

5. Sakurai, A., "Blast Wave Theory," Basic Developments in Fluid Dynamics, Vol. I, Academic Press, pp. 309, (1965).

6. Unwin, J. J., "The Production of Wave by the Sudden Release of a Spherical Distribution of Compressed Air in the Atmosphere," Proc. Roy. Soc. A178, (1941).

7. Roberts, L., "On the Numerical Solution of the Equations for a Spherica. Wave of Finite Amplitude, II," Jl. Math. and Phys., Vol. 36, No. 4, (Jan. 1958).

8. Whitham, G. B., "The Propagation of Spherical Blast," Proc. Roy. Soc. (London, 1950).

9. Von Neumann, J., and Richtmyer, R. D., "A Method for the Numerical Calculation of Hydrodynamic Shocks," Jl. Applied Phys., (1950).

10. Wecken, F., "Expansion of a High Pressure Gas Sphere," Z. Angew. Math., (1950).

11. Schardin, H., "Measurement of Spherical Shock Waves," Commu. Pure and Applied Math., Vol. VII, (1954).

12. Fox, P., and Ralston, A., "On the Solution of the Equations for Spherical Waves of Finite Amplitude I," J. Math. and Phys., Vol. 36, No. 4, (Jan. 1958).

13. Zhukov, A. I., "Application of the Method of Characteristics to the Numerical Solution of One Dimensional Problems in Gas Dynamics," Math. Inst. Akad. Nuak S. S. S. R. No. 58, (1960).

14. Hartree, D. R., "Numerical Analysis," Oxford Univ. Press, (1958).

15. Hoskin, N. E., "Method in Computational Physics," (Alder, B., Fernbach, S., and Rotenberg, M., eds.) Vol. 3, pp. 288, Academic Press, New York, (1964).

16. Lister, M., in "Mathematical Methods for Digital Computers," (Ralston, A., and Wilf, H. S., eds.) Sec. 15, Wiley, New York, (1960).

17. Katskova, O. N., and Chuskin, P. I., "A Scheme for the Numerical Method of Characteristics," Dokl. Akad. Nauk S. S. S. R., (1964).

18. McFadden, J. A., "Initial Behavior of a Spherical Blast," J. Applied Phys., (1952).

19. Berry, F. J., and Holt, M., "The Initial Propagation of Spherical Blast from Certain Explosives," Proc. Roy. Soc. A224, (1954).

20. Berry, F. F., Bulter, D. S., and Holt, M., "The Early Development of Spherical Blast from a Particular Charge," Proc. Roy. Soc. A227, (1954-1955).

21. Von Mises, R., "Mathematical Theory of Compressible Fluid Flow," Academic Press Inc., New York, pp. 100-112.

22. Courant, R., and Friedrichs, K. O., "Supersonic Flow and Shock Waves," (Interscience Publishers, New York, 1948).

23. Chou, P. C., and Karpp, R. R., "Solution of Blast Wave by the Method of Characteristics," DIT Report No. 125-7, September 1965.

24. Chou, P. C., Karpp, R. R., and Huang, S. L., "Numerical Calculation of Blast Waves by the Method of Characteristics," AIAA Journal, Vol. 5, No. 4, pp. 618-623, April 1967.

25. Huang, S. L., and Chou, P. C., "Solution of Blast Waves by a Constant Time Scheme in the Method of Characteristics," DIT Report No. 125-9, August 1966.

26. Brode, H. L., "The Blast from a Sphere of High Pressure Gas," Rand Corp. Report P-582, (1955).

27. Walsh, J. M., Johnson, W. E., Dienes, J. K., Tillotson, J. H., and Yates, D. R., "Summary Report on the Theory of Hypervelocity Impact," GA-5119, General Atomic, General Dynamics, San Diego, California, March 1964.

28. Chou, P. C., and Burns, B. P., "Late-Stage Equivalence in One-Dimensional Impacts," DIT Report No. 125-8, (1966), and Journal of Applied Physics, Vol. 38, No. 2, pp. 553-560, February 1967.

29. Riney, T. D., and Heyda, J. F., "Hypervelocity Impact Calculations," Seventh Hypervelocity Impact Symposium, Vol. II-Theory, (1965).

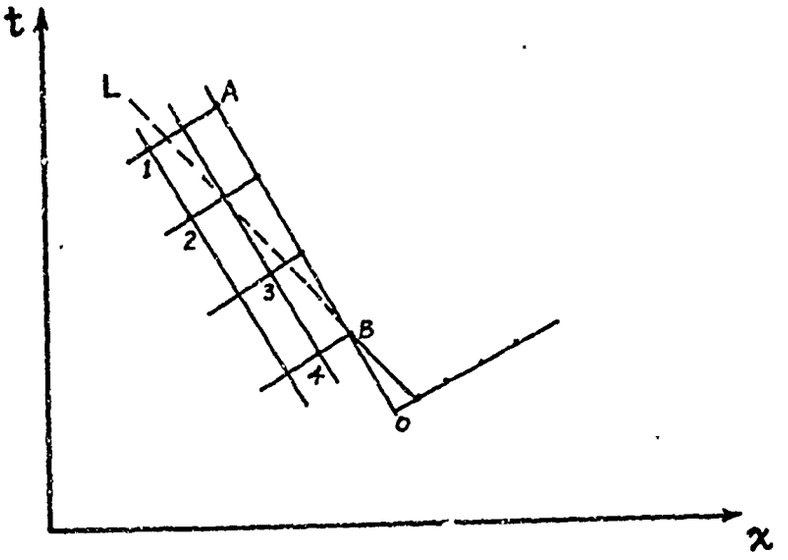

Figure 1 Shock Propagates into Region Over-determined by Characteristic Net

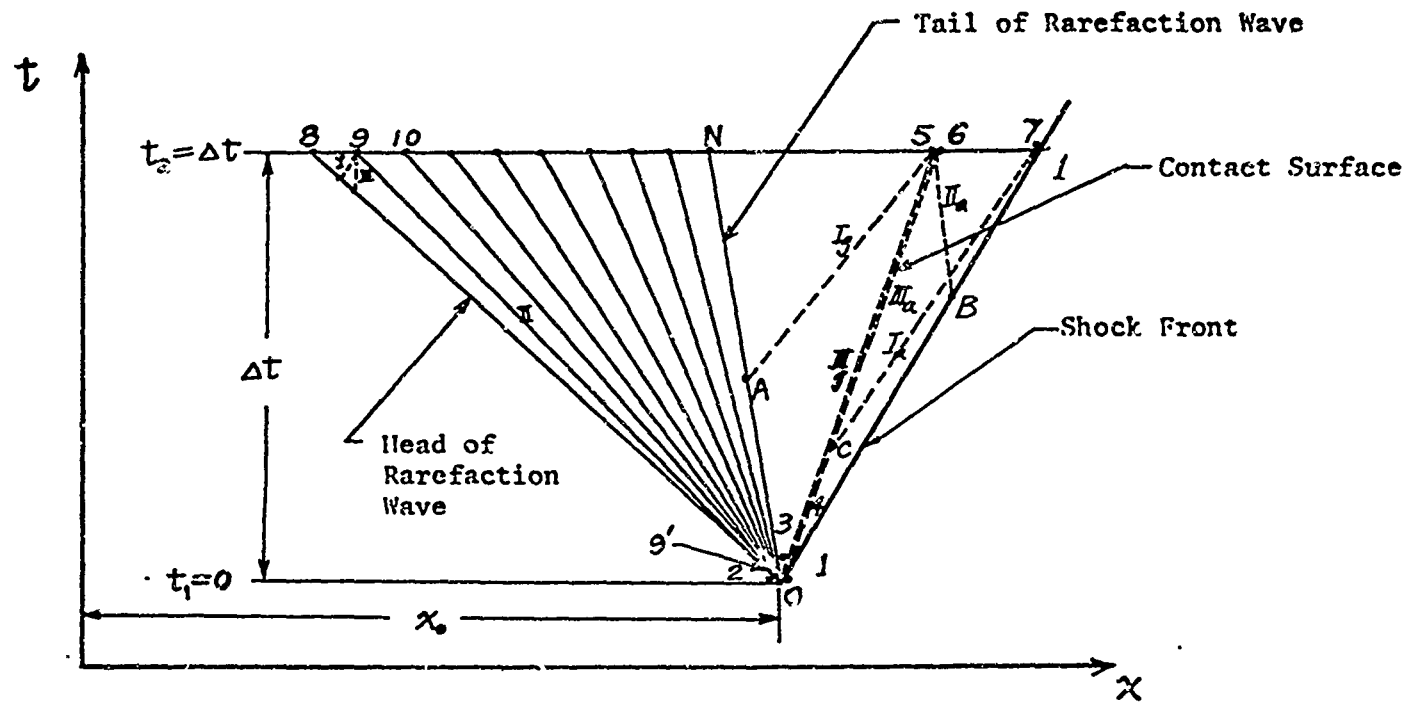

Figure 2 Initial Singularity

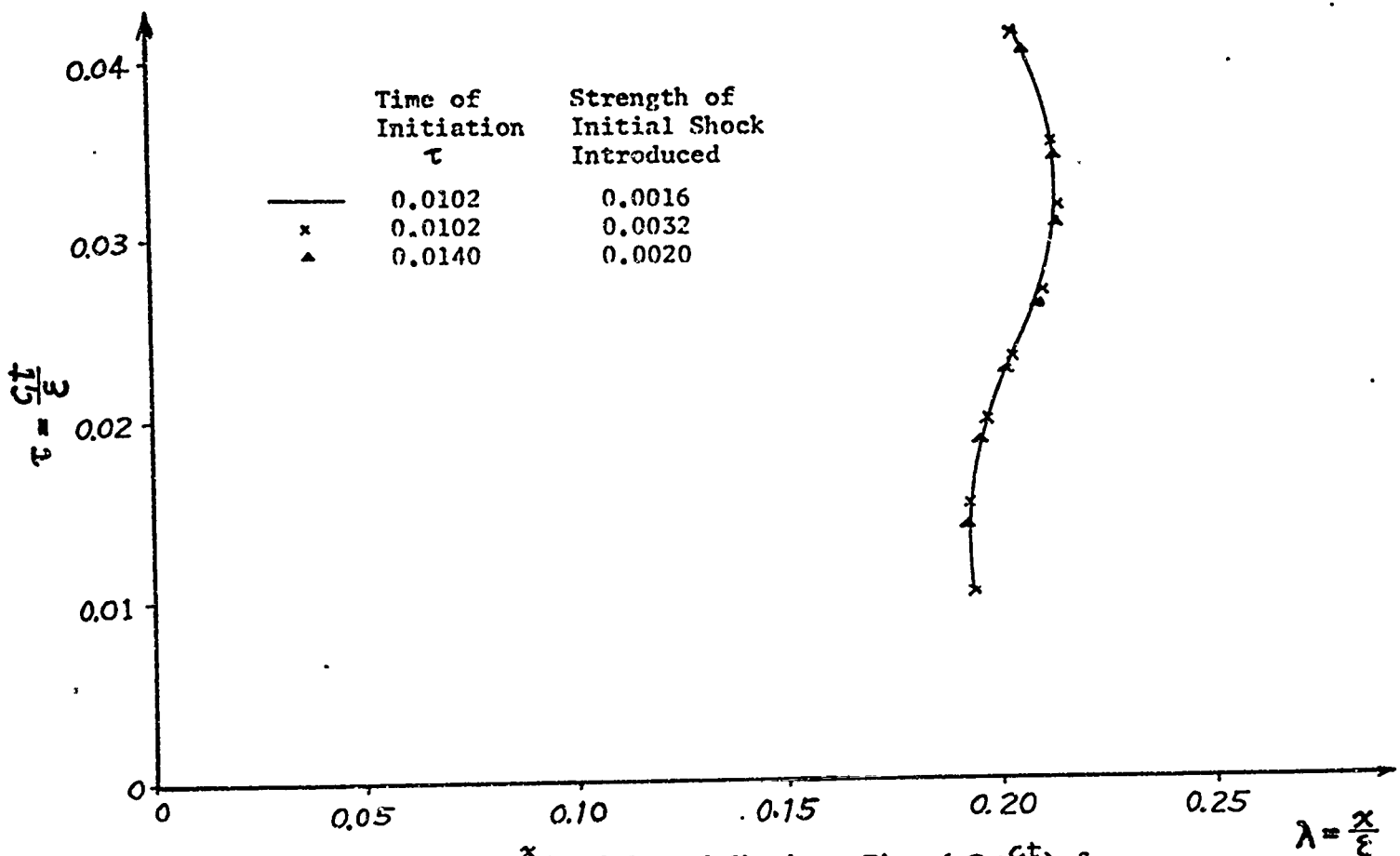

Figure 3 Position ($\lambda = \frac{x}{\varepsilon}$) of Second Shock vs Time ($\tau = \frac{ct}{\varepsilon}$) for Different Initiation Conditions ($\pi_0 = 100$, $\eta_0 = 1.16$, $\gamma_2 = 1.4$)

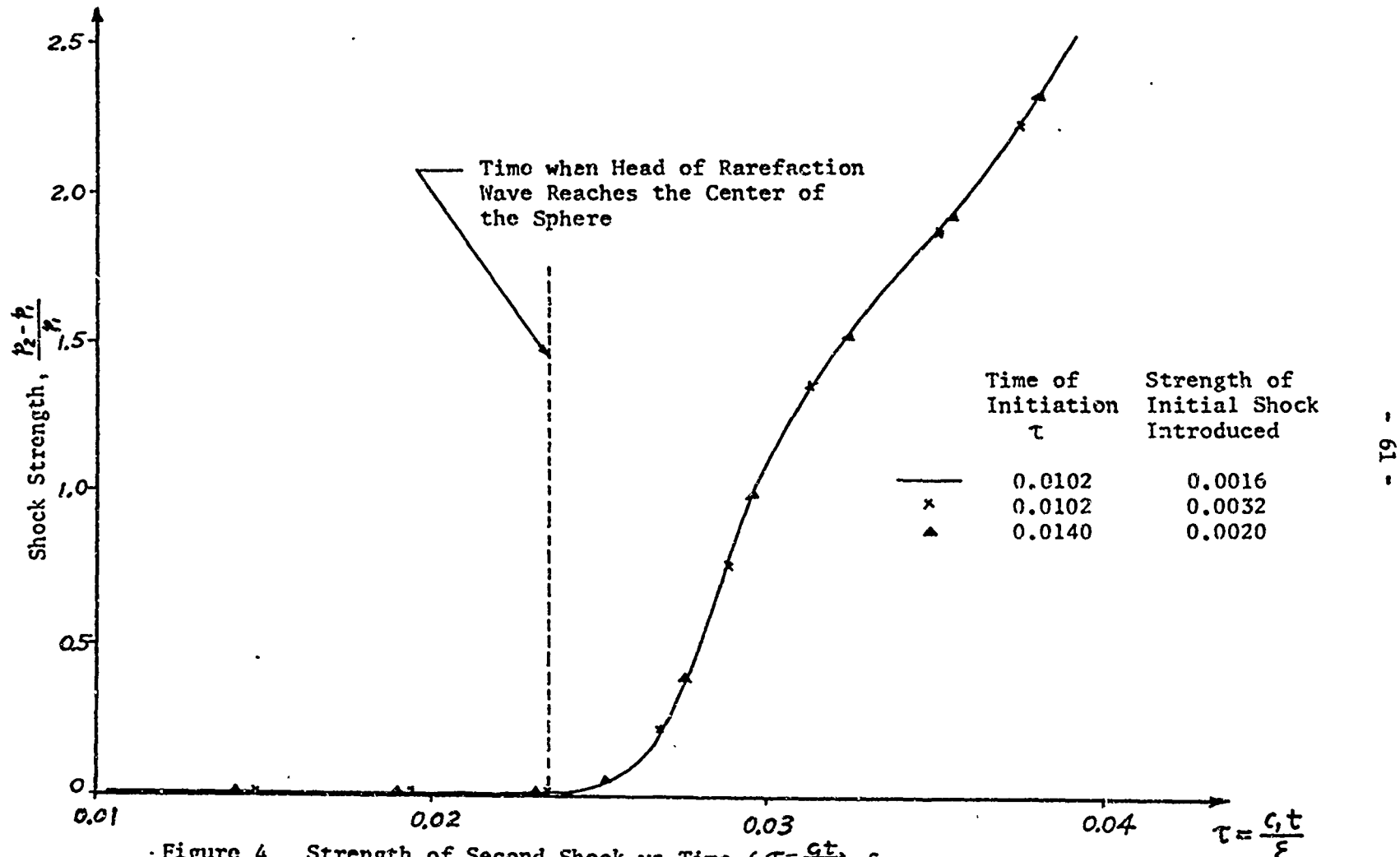

Figure 4 Strength of Second Shock vs Time ($\tau = \frac{c_1 t}{\varepsilon}$) for Different Initiation Conditions ($\pi_1 = 100$, $\gamma_1 = 1.16$, $\gamma_2 = 1.4$)

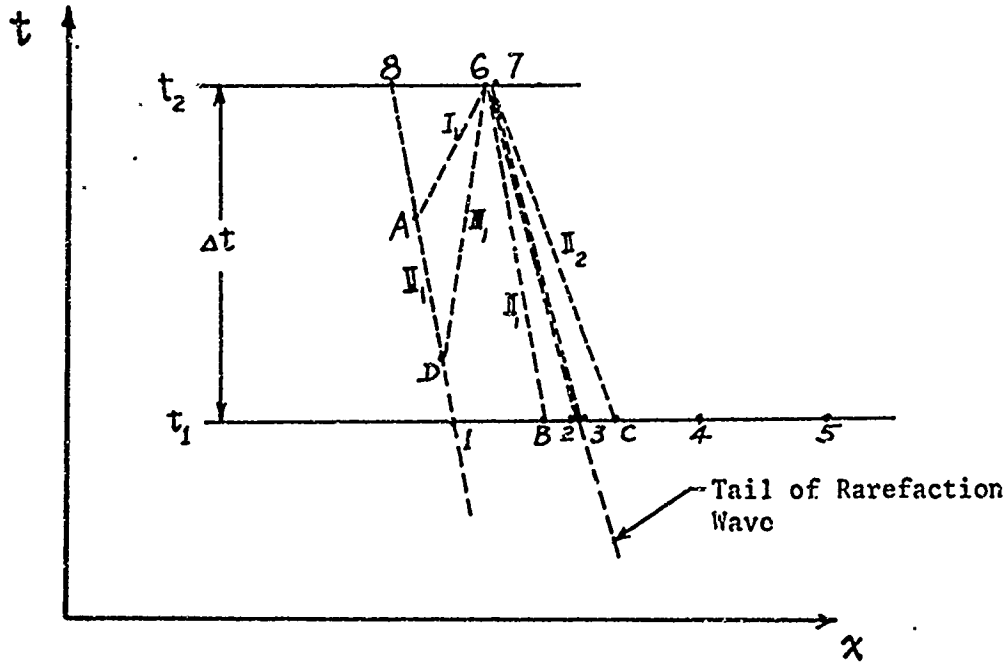

Figure 5 Initiation of Second Shock

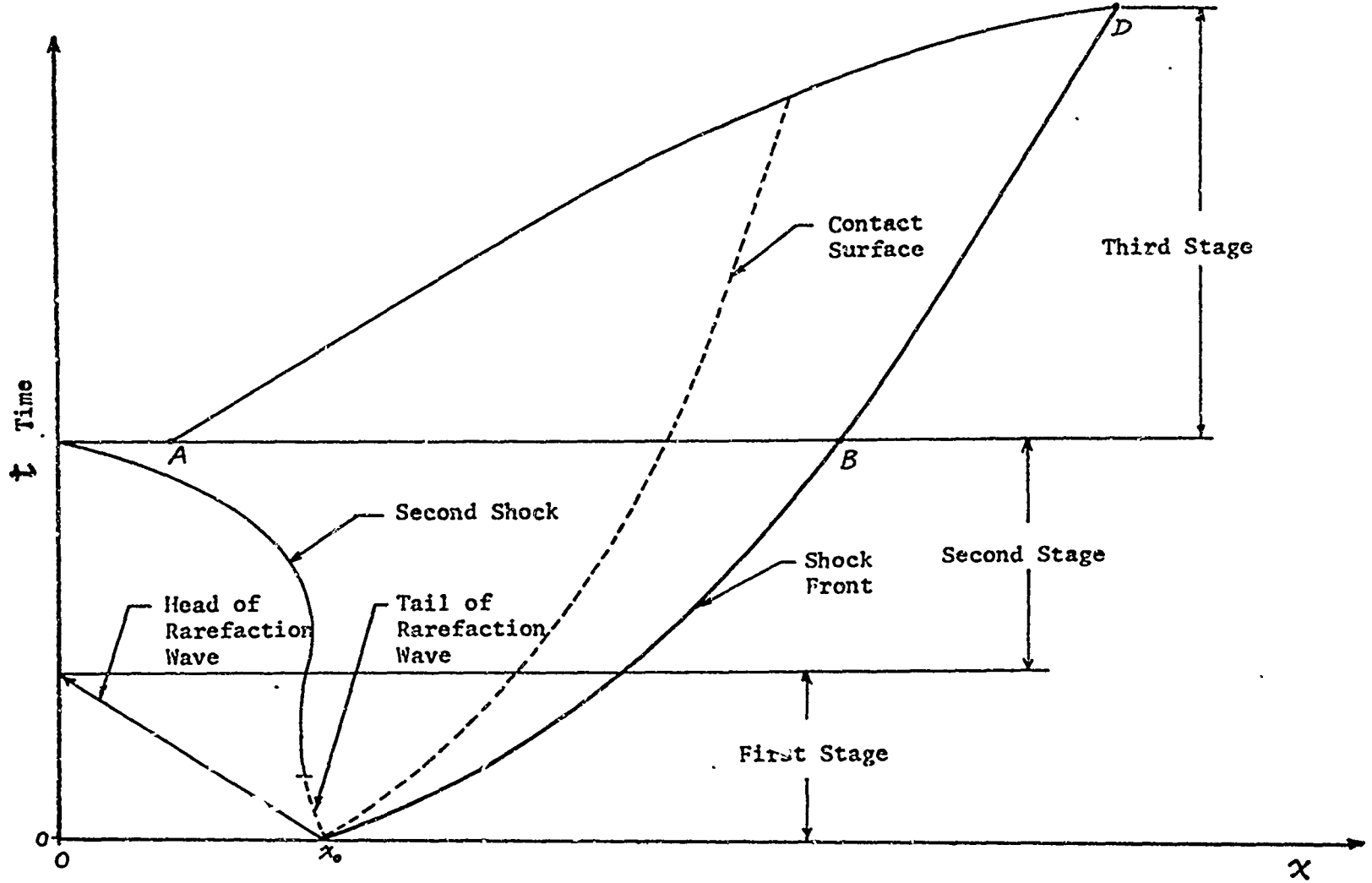

Figure 6 Schematic of Region of Numerical Solution

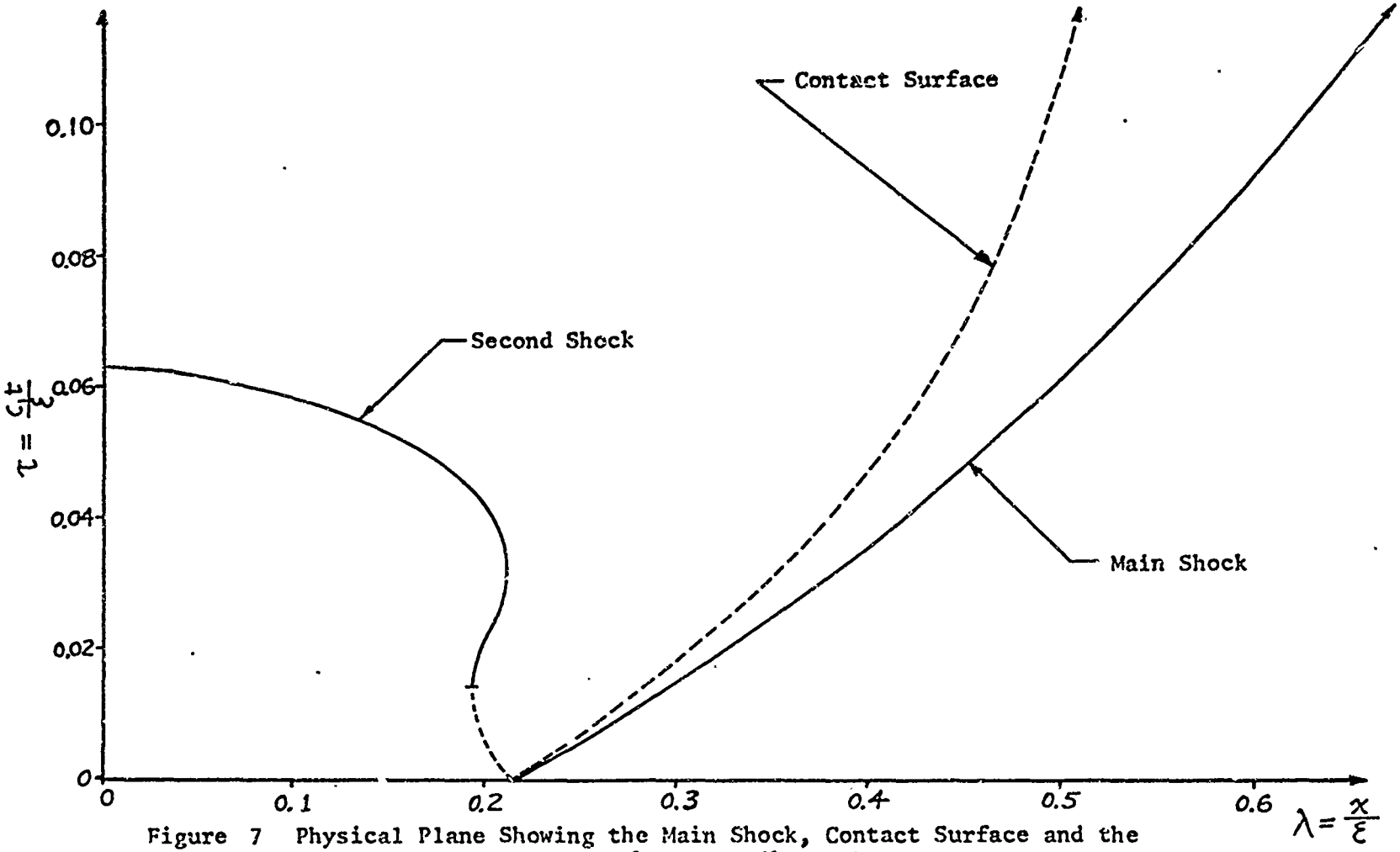

Figure 7 Physical Plane Showing the Main Shock, Contact Surface and the Second Shock ($\pi_0 = 100$, $\eta_0 = 1.16$, $\gamma_2 = 1.4$)

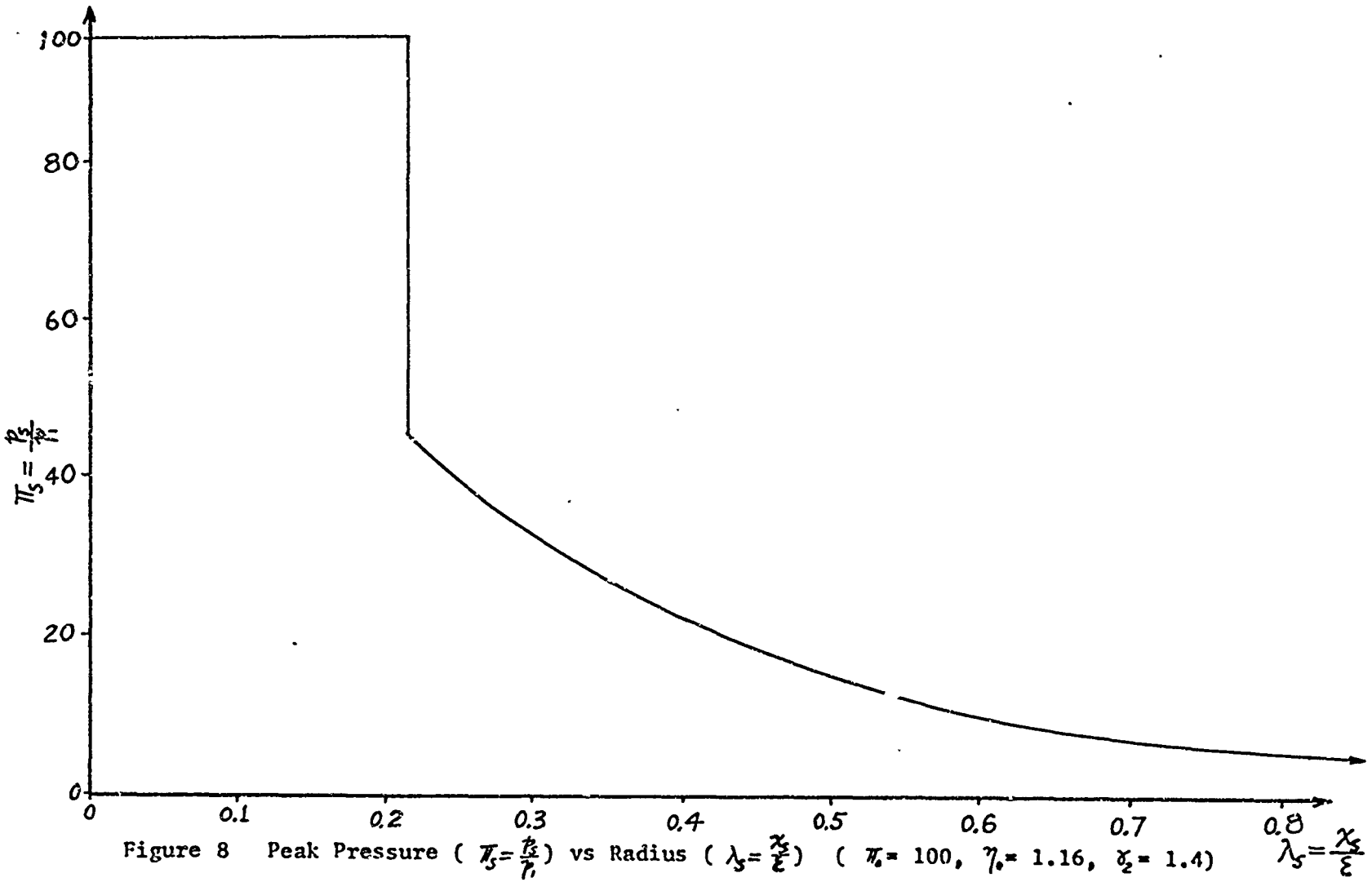

Figure 8 Peak Pressure ($\pi_s = \frac{p_s}{p_1}$) vs Radius ($\lambda_s = \frac{x_s}{\xi}$) ($\pi_0 = 100$, $\gamma_0 = 1.16$, $\gamma_2 = 1.4$)

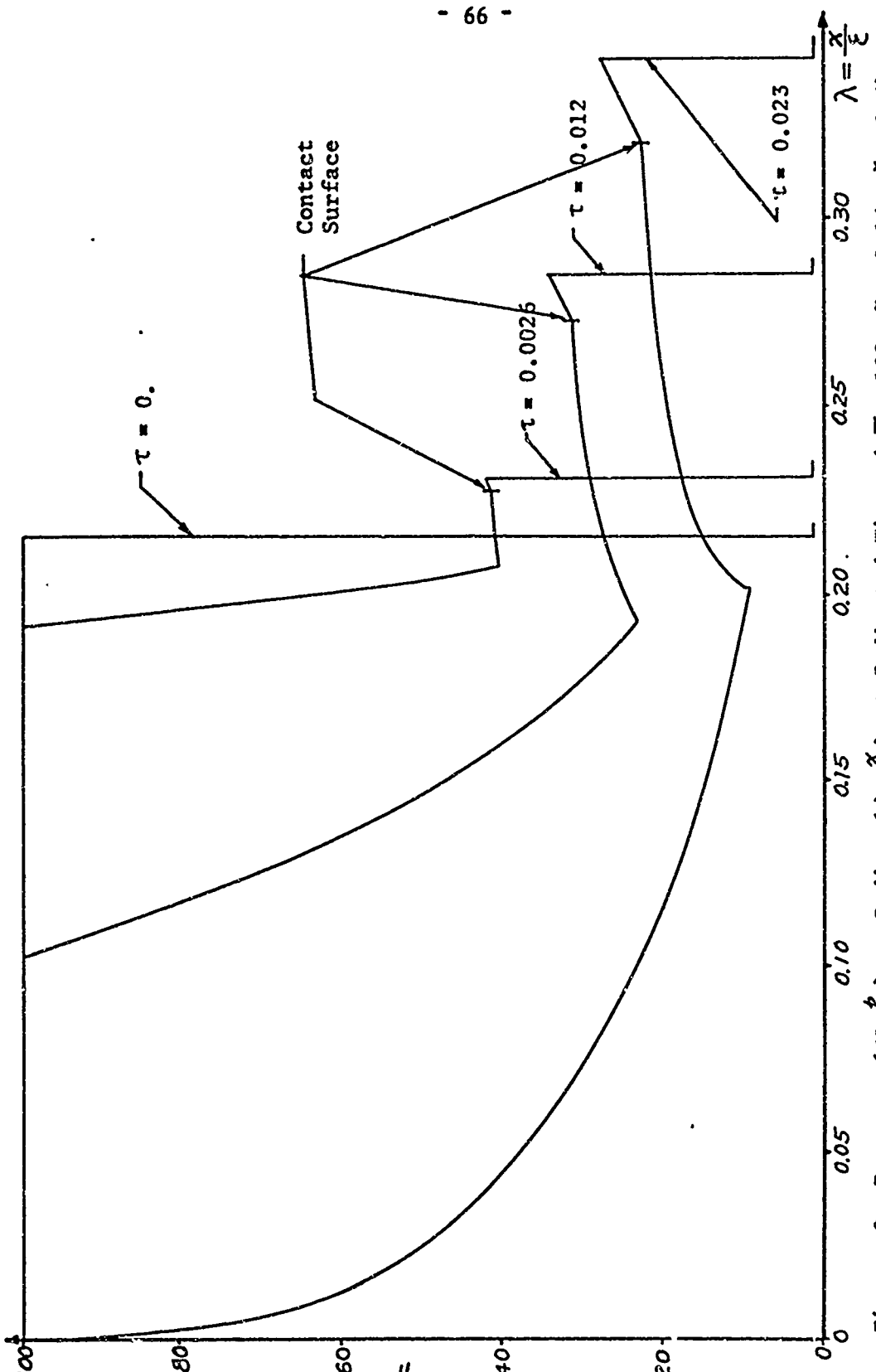

Figure 9 Pressure ($\Pi = \frac{p}{p_1}$) vs Radius ($\lambda = \frac{x}{\xi}$) at Indicated Times ($\gamma_1 = 100$, $\gamma_0 = 1.16$, $\gamma_2 = 1.4$)

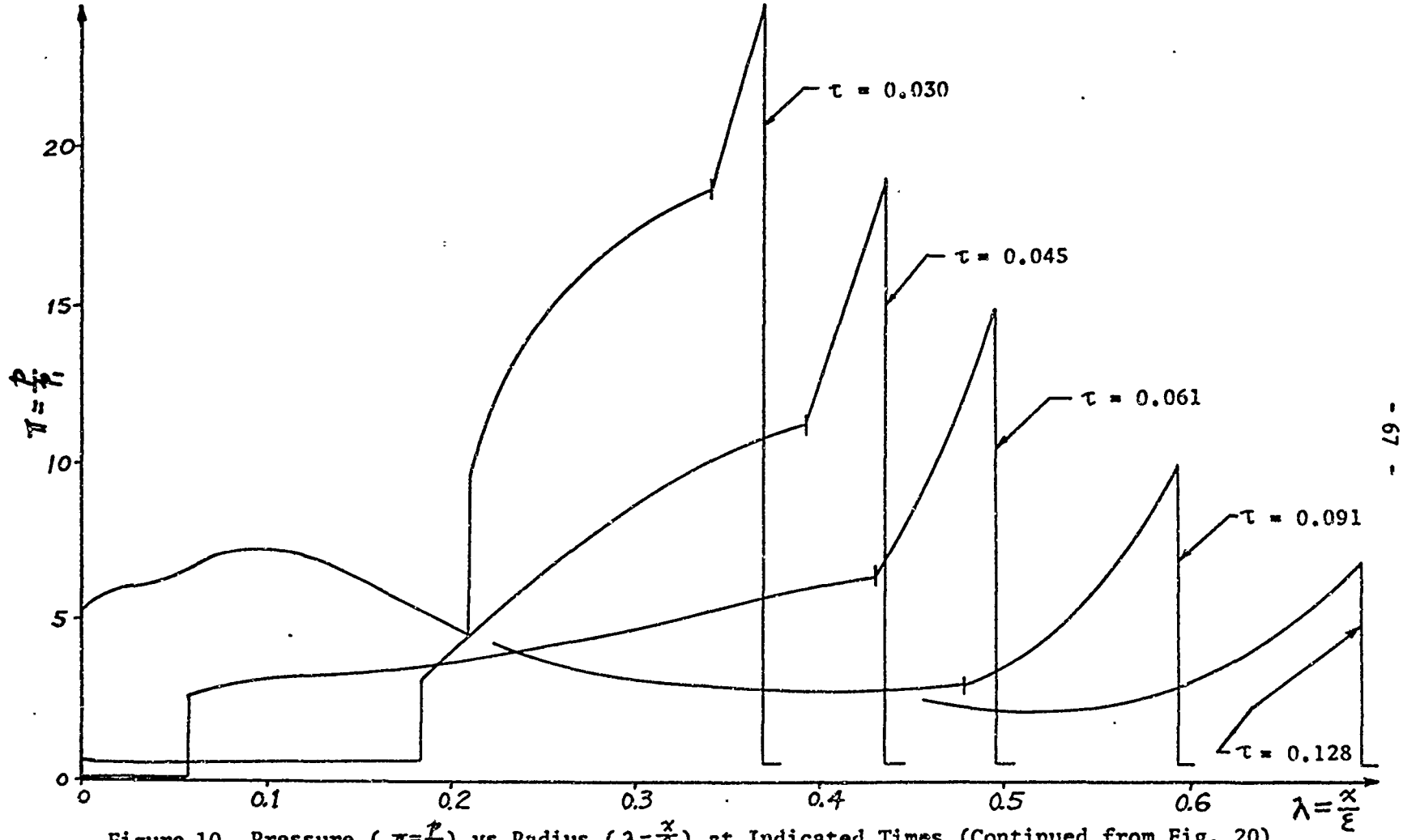

Figure 10 Pressure ($\pi = \frac{p}{p_i}$) vs Radius ($\lambda = \frac{x}{\varepsilon}$) at Indicated Times (Continued from Fig. 20)
($\pi_0 = 100$, $\eta_0 = 1.16$, $\gamma_2 = 1.4$)

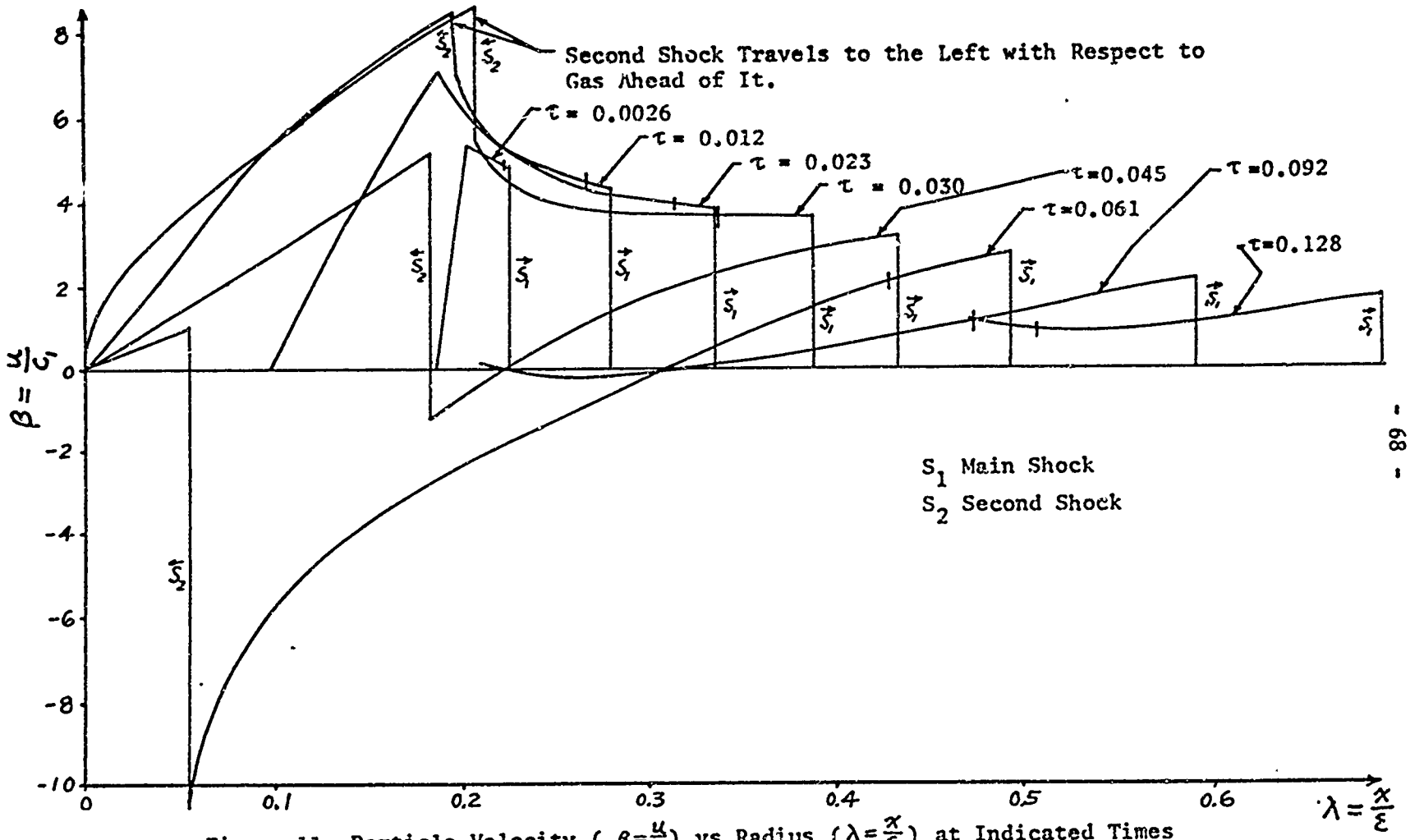

Figure 11 Particle Velocity ($\beta=\frac{u}{c_1}$) vs Radius ($\lambda=\frac{x}{\varepsilon}$) at Indicated Times
($\pi_0 = 100$, $\eta_0 = 1.16$, $\gamma_2 = 1.4$)

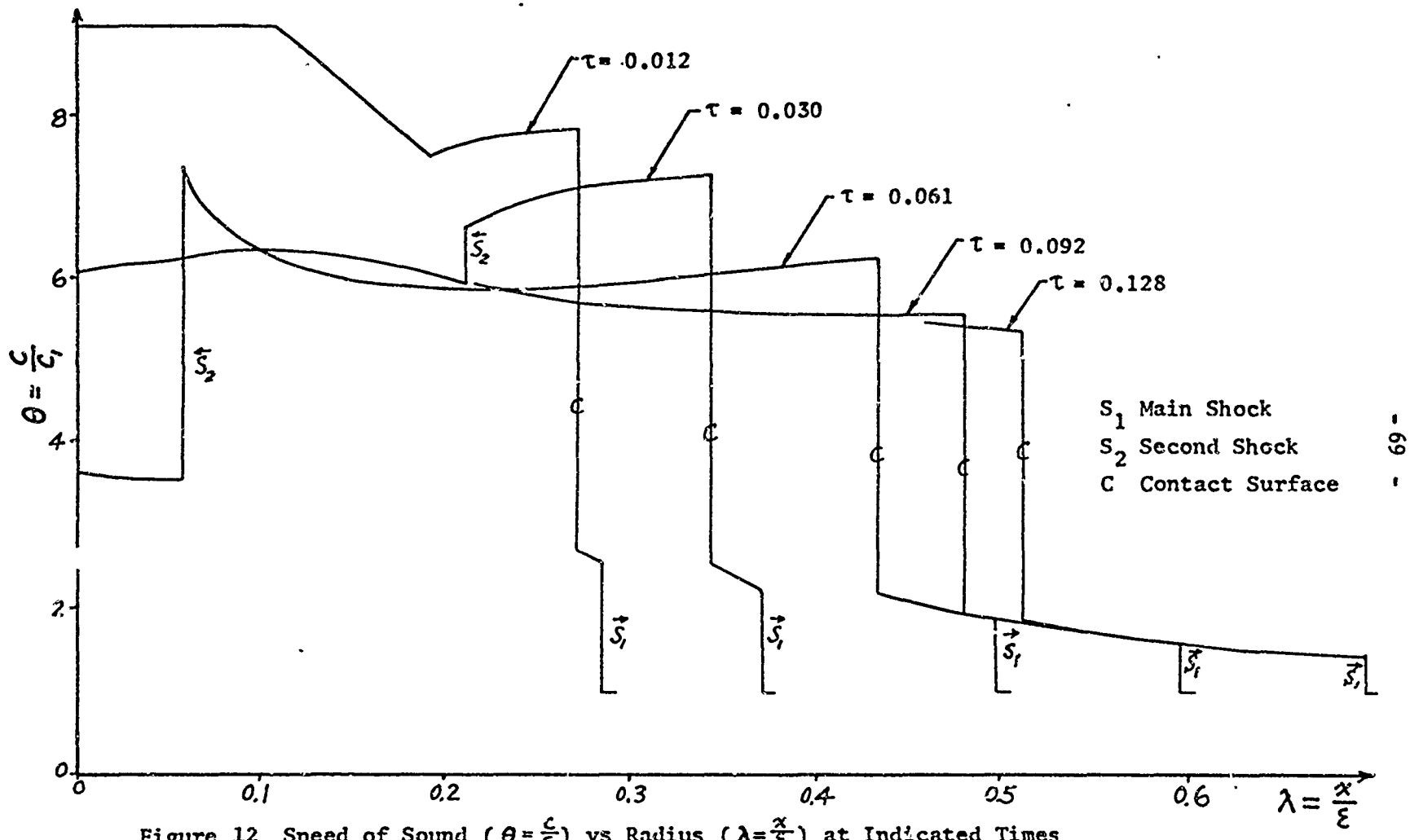

Figure 12 Speed of Sound ($\theta = \frac{c}{c_1}$) vs Radius ($\lambda = \frac{x}{\varepsilon}$) at Indicated Times
($\pi_0 = 100$, $\eta_0 = 1.16$, $\gamma_2 = 1.4$)

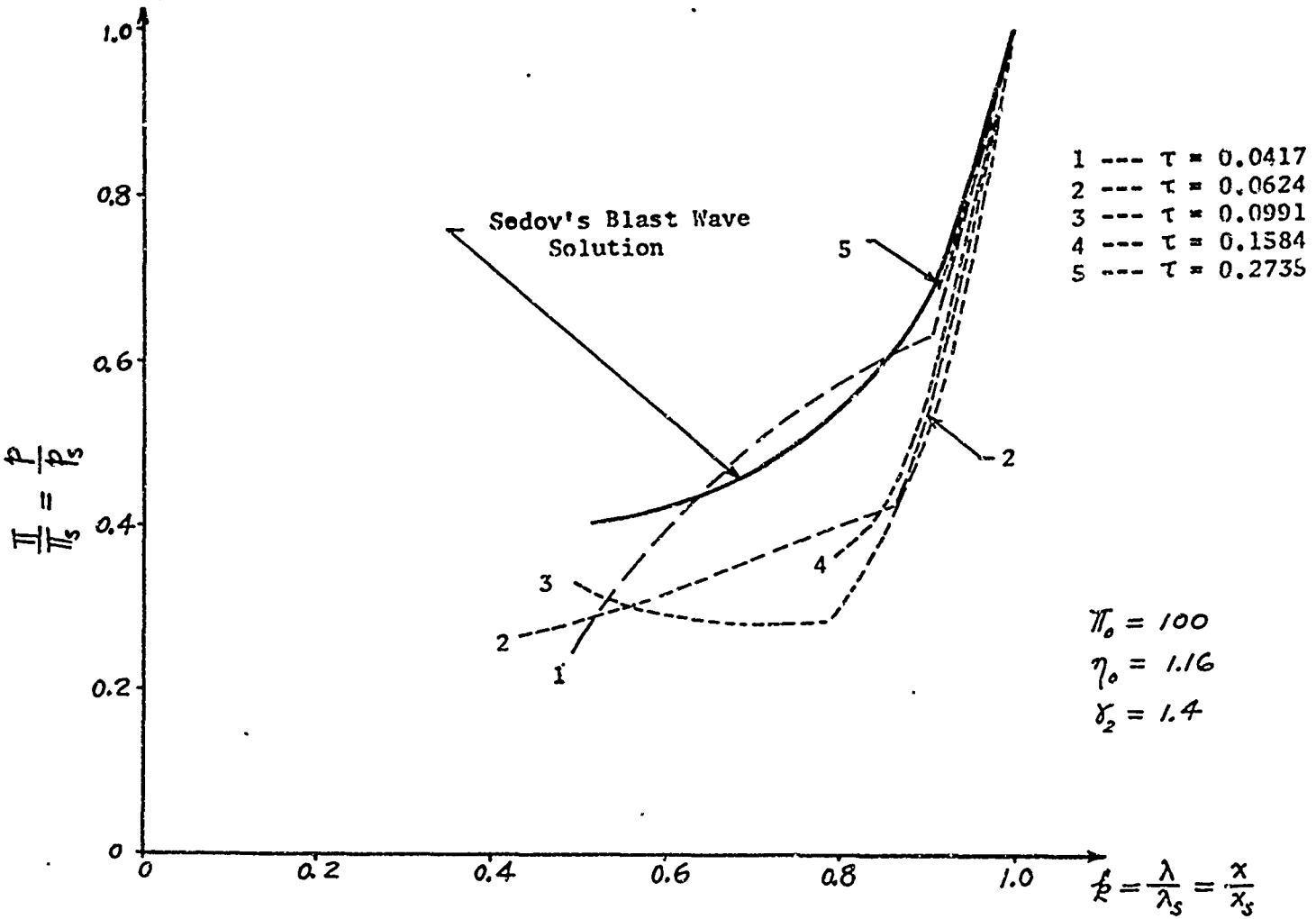

Figure 13 Pressure Ratio ($\frac{\Pi}{\Pi_s}=\frac{P}{P_s}$) vs Radius Ratio ($\xi=\frac{\lambda}{\lambda_s}$) at Indicated Times

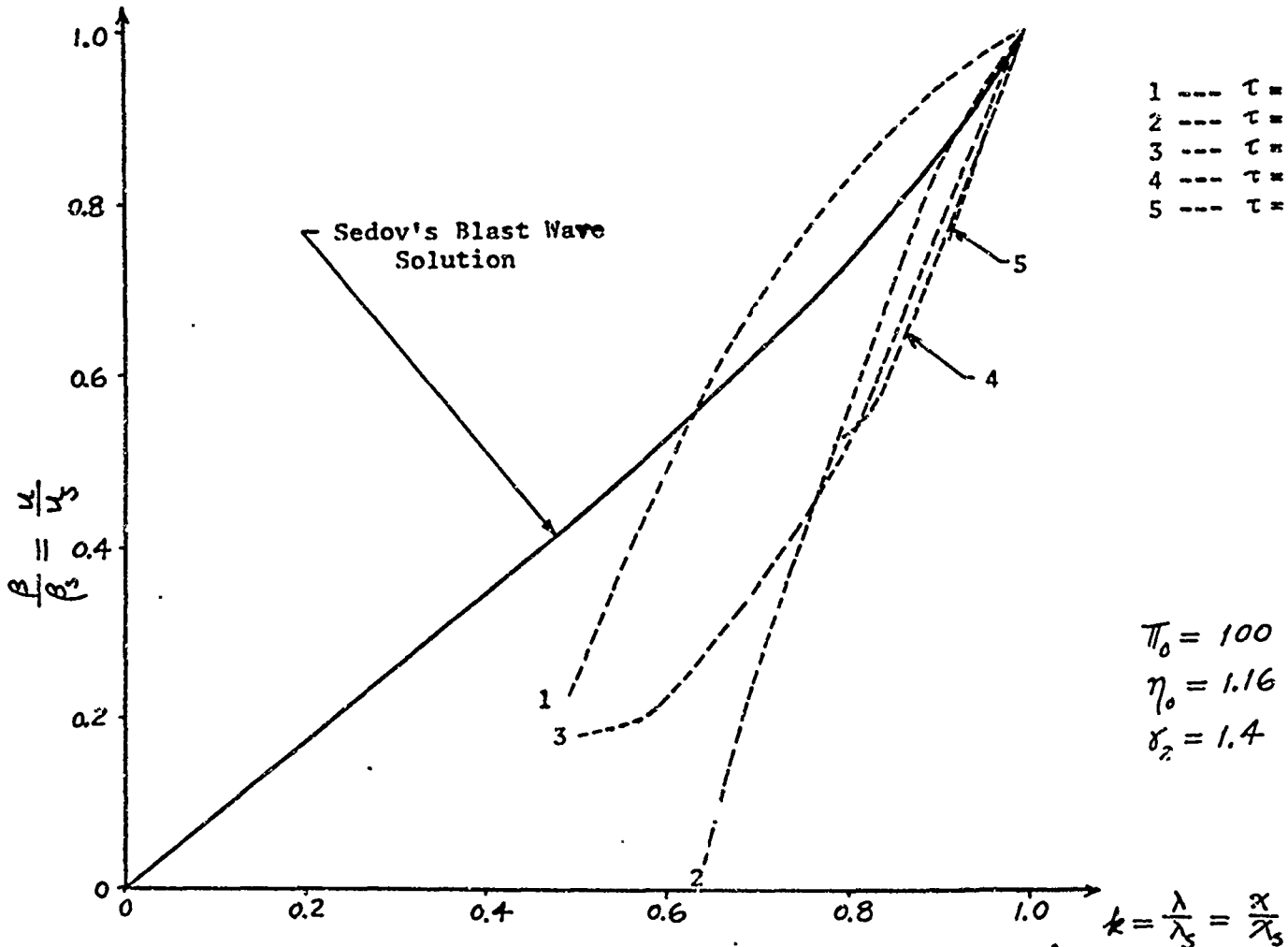

Figure 14 Particle Velocity Ratio ($\frac{\beta}{\beta_s}=\frac{u}{u_s}$) vs Radius Ratio ($k=\frac{\lambda}{\lambda_s}$) at Indicated Times

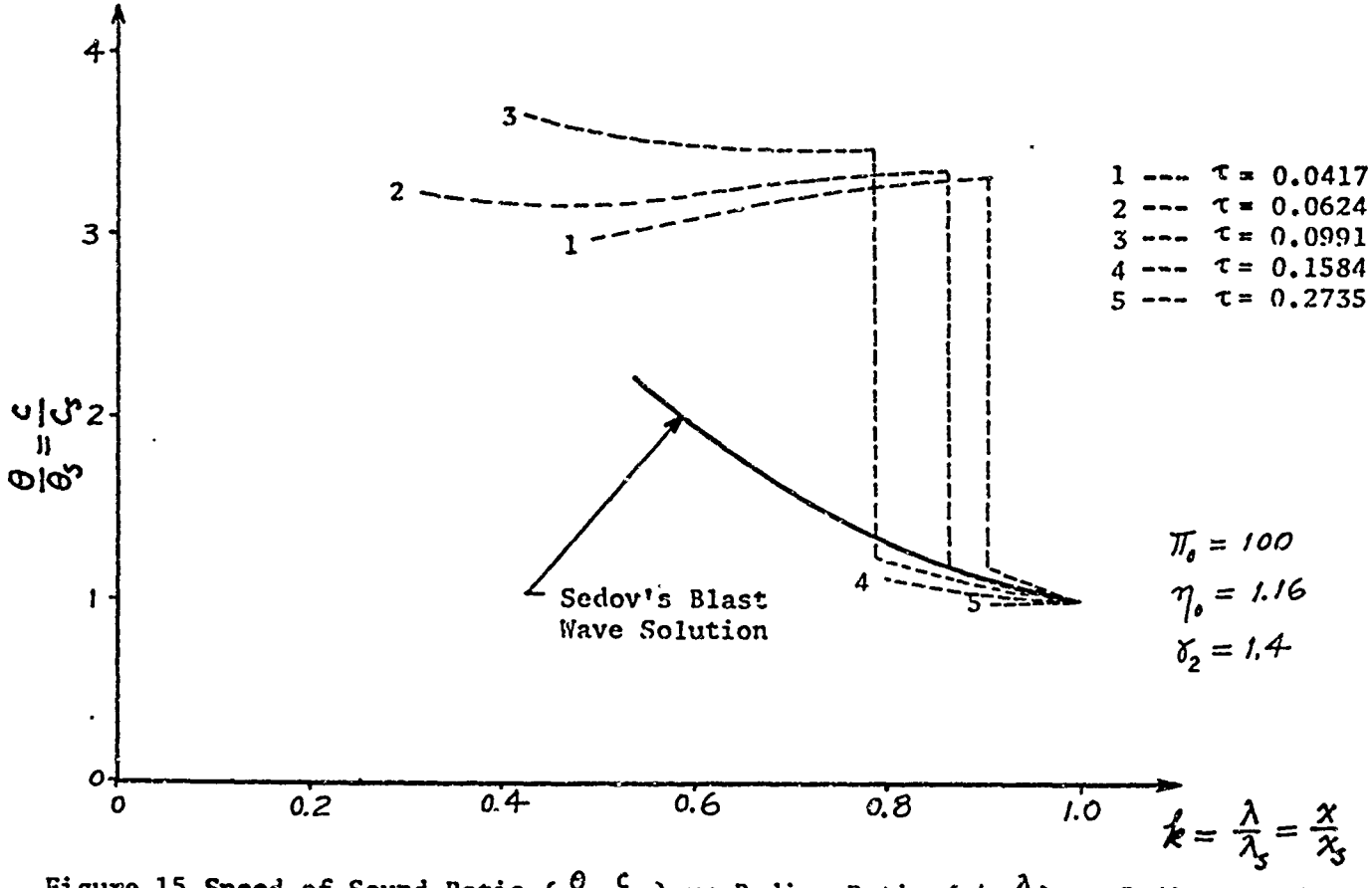

Figure 15 Speed of Sound Ratio ($\frac{\theta}{\theta_s}=\frac{c}{c_s}$) vs Radius Ratio ($k=\frac{\lambda}{\lambda_s}$) at Indicated Times

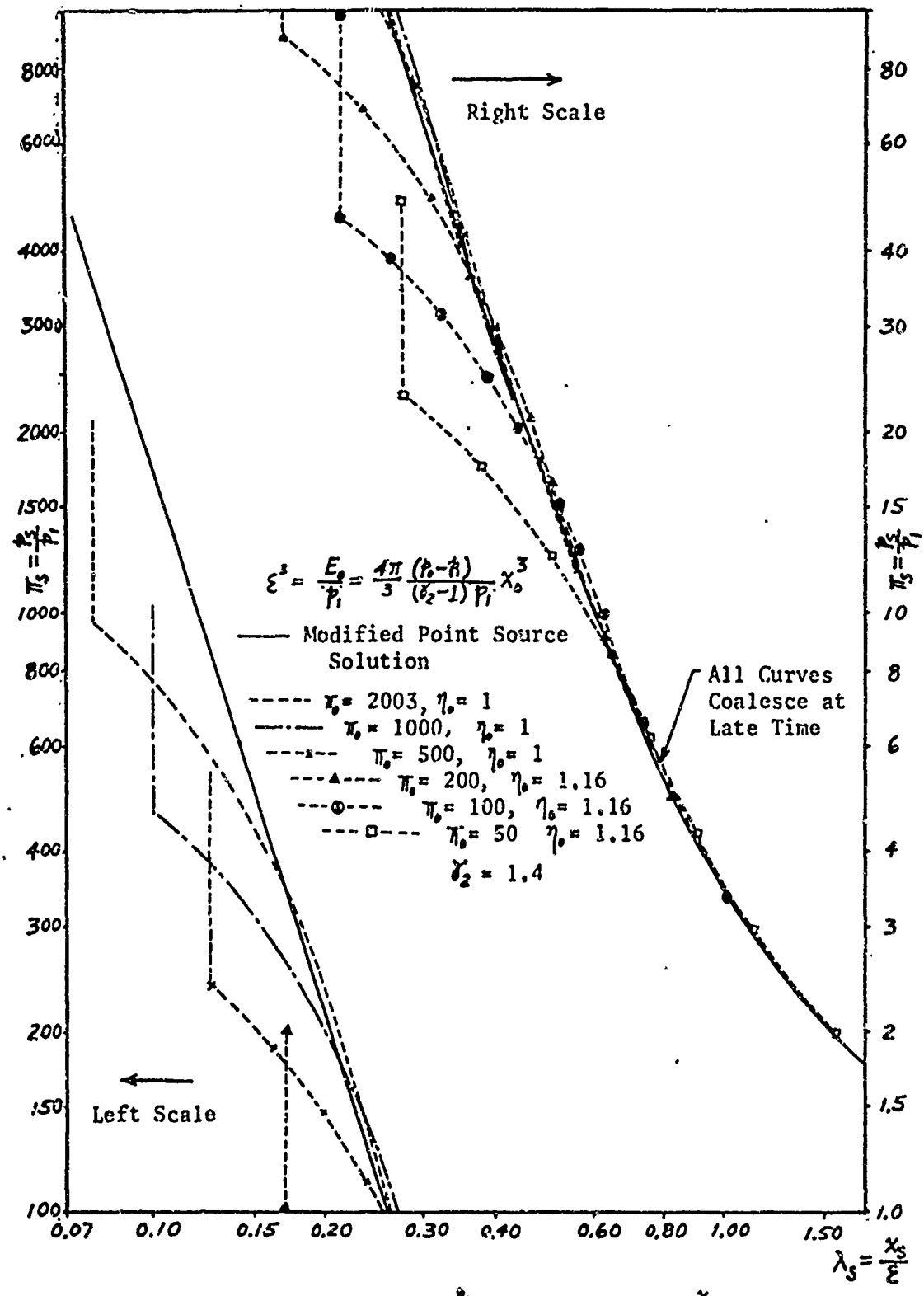

Figure 16 Peak Pressure ($\pi_s = \frac{p_s}{p_1}$) vs Radius ($\lambda_s = \frac{\chi_s}{\varepsilon}$) for Expanding Spheres with Equal Initial Energy, but Different Initial Pressure Density and Radius

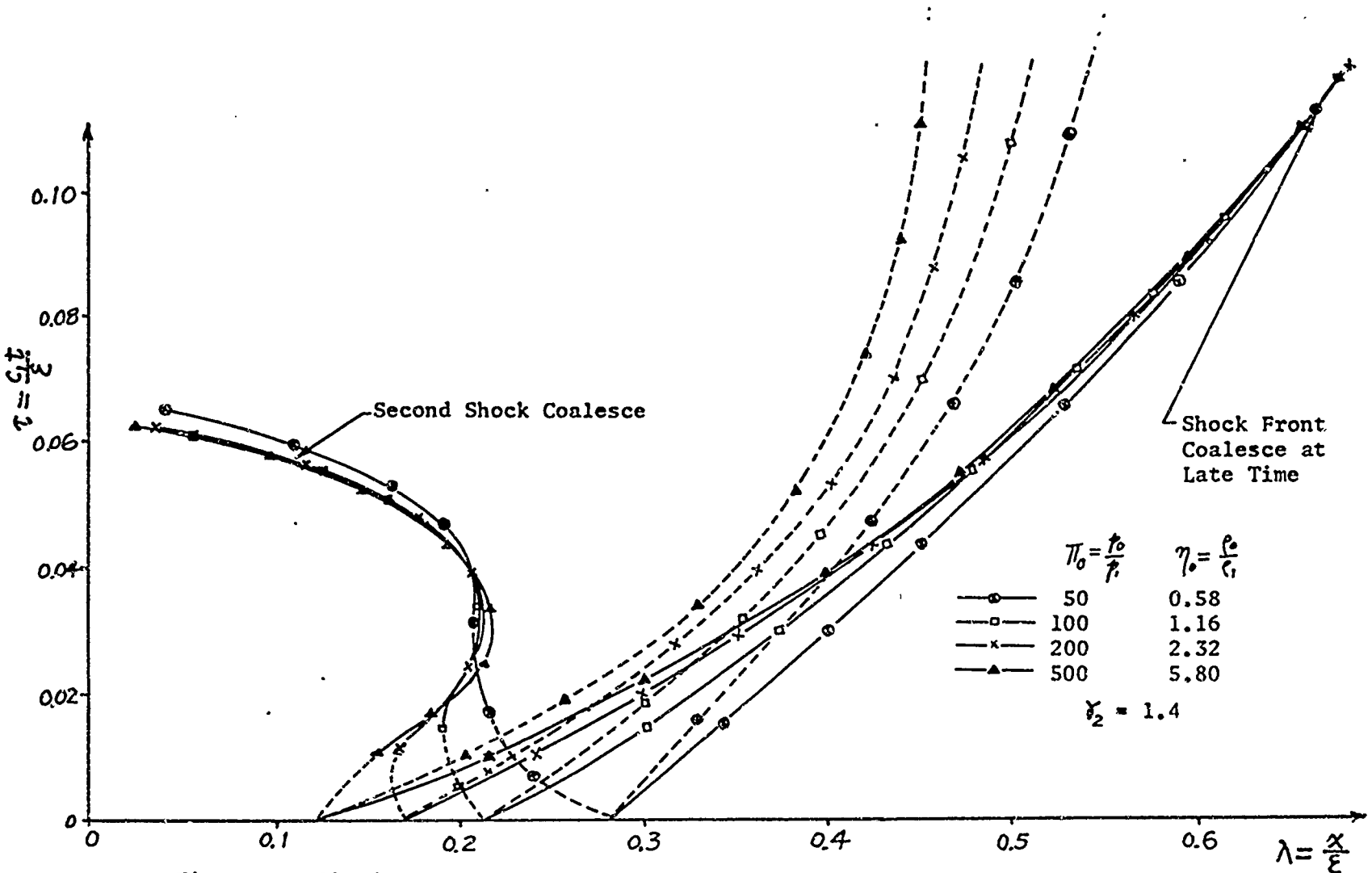

Figure 17 Physical Plane (λ-τ) Showing Shock Front, Contact Surface and Second Shock for Cases with Equal Initial Energy and Equal Initial Mass

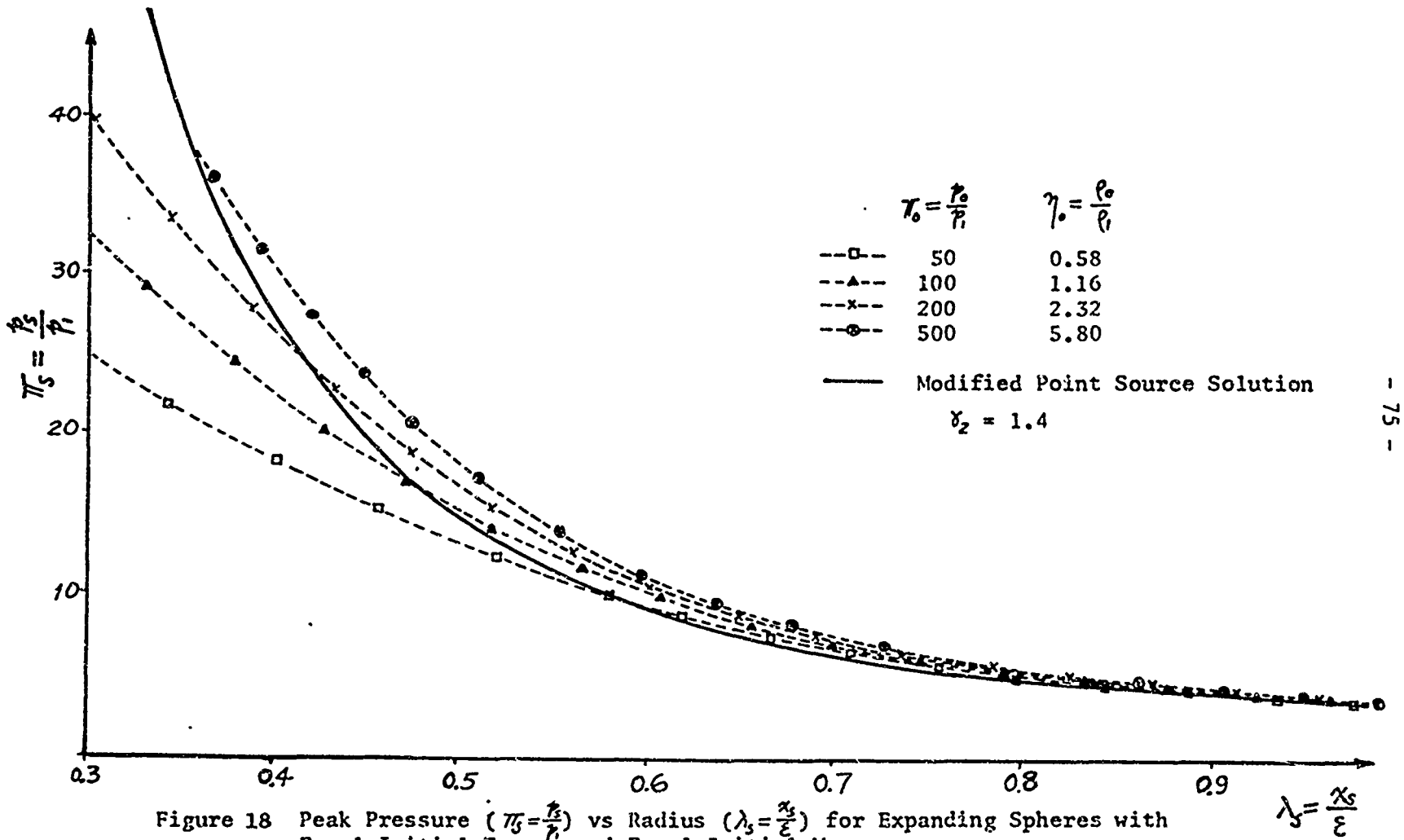

Figure 18 Peak Pressure ($\pi_s = \frac{p_s}{p_1}$) vs Radius ($\lambda_s = \frac{x_s}{\varepsilon}$) for Expanding Spheres with Equal Initial Energy and Equal Initial Mass

Unclassified

Security Classification

DOCUMENT CONTROL DATA - R&D

(Security classification of title, body of abstract and indexing annotation must be entered when the overall report is classified)

1. ORIGINATING ACTIVITY *(Corporate author)*

Drexel Institute of Technology
Philadelphia, Pennsylvania

2a. REPORT SECURITY CLASSIFICATION

Unclassified

2b GROUP

3. REPORT TITLE

CALCULATIONS OF EXPANDING SHOCK WAVES AND LATE-STAGE EQUIVALENCE

4. DESCRIPTIVE NOTES *(Type of report and inclusive dates)*

5. AUTHOR(S) *(Last name, first name, initial)*

Huang, Shih L., and Chou, Pei C.

6. REPORT DATE	7a. TOTAL NO. OF PAGES	7b. NO. OF REFS
April 1968	75	29

8a. CONTRACT OR GRANT NO.	9a. ORIGINATOR'S REPORT NUMBER(S)
DA-18-001-AMC-876(X)	
b. PROJECT NO.	125-12
c.	9b. OTHER REPORT NO(S) *(Any other numbers that may be assigned this report)*
d.	

10. AVAILABILITY/LIMITATION NOTICES

This document has been approved for public release and sale; its distribution is unlimited.

11. SUPPLEMENTARY NOTES	12. SPONSORING MILITARY ACTIVITY
	U.S. Army Ballistics Research Laboratory Aberdeen Proving Ground, Maryland

13. ABSTRACT

A numerical scheme based on the method of characteristics is developed and applied to the flow field of the expansion of a high pressure sphere into atmosphere. It is shown that this method is very accurate, involving errors of less than 1%. In calculating the expanding sphere, two rather challenging problems, namely, the initial singularity and the formation of a second shock, are successfully solved through special techniques. (U)

The formation of an inward traveling shock, in addition to the main shock, is found to exist at the tail of the left traveling rarefaction wave. The strength of the second shock remains rather weak at the early stage of its development, it becomes very strong just before reaching the center of the sphere. (U)

It is shown that "late-stage equivalence" exists in the expansion of high pressure spheres into atmosphere, provided the initial total energy in each of the spheres is held constant. Late-stage equivalence is assumed to exist if the peak pressure distribution for different expanding spheres are the same for long times. (U)

DD FORM 1 JAN 64 1473

Unclassified

Security Classification

14. KEY WORDS	LINK A		LINK B		LINK C	
	ROLE	WT	ROLE	WT	ROLE	WT

INSTRUCTIONS

1. ORIGINATING ACTIVITY: Enter the name and address of the contractor, subcontractor, grantee, Department of Defense activity or other organization *(corporate author)* issuing the report.

2a. REPORT SECURITY CLASSIFICATION: Enter the overall security classification of the report. Indicate whether "Restricted Data" is included. Marking is to be in accordance with appropriate security regulations.

2b. GROUP: Automatic downgrading is specified in DoD Directive 5200.10 and Armed Forces Industrial Manual. Enter the group number. Also, when applicable, show that optional markings have been used for Group 3 and Group 4 as authorized.

3. REPORT TITLE: Enter the complete report title in all capital letters. Titles in all cases should be unclassified. If a meaningful title cannot be selected without classification, show title classification in all capitals in parenthesis immediately following the title.

4. DESCRIPTIVE NOTES: If appropriate, enter the type of report, e.g., interim, progress, summary, annual, or final. Give the inclusive dates when a specific reporting period is covered.

5. AUTHOR(S): Enter the name(s) of author(s) as shown on or in the report. Enter last name, first name, middle initial. If military, show rank and branch of service. The name of the principal author is an absolute minimum requirement.

6. REPORT DATE: Enter the date of the report as day, month, year, or month, year. If more than one date appears on the report, use date of publication.

7a. TOTAL NUMBER OF PAGES: The total page count should follow normal pagination procedures, i.e., enter the number of pages containing information.

7b. NUMBER OF REFERENCES: Enter the total number of references cited in the report.

8a. CONTRACT OR GRANT NUMBER: If appropriate, enter the applicable number of the contract or grant under which the report was written.

8b, 8c, & 8d. PROJECT NUMBER: Enter the appropriate military department identification, such as project number, subproject number, system numbers, task number, etc.

9a. ORIGINATOR'S REPORT NUMBER(S): Enter the official report number by which the document will be identified and controlled by the originating activity. This number must be unique to this report.

9b. OTHER REPORT NUMBER(S): If the report has been assigned any other report numbers *(either by the originator or by the sponsor)*, also enter this number(s).

10. AVAILABILITY/LIMITATION NOTICES: Enter any limitations on further dissemination of the report, other than those imposed by security classification, using standard statements such as:

(1) "Qualified requesters may obtain copies of this report from DDC."

(2) "Foreign announcement and dissemination of this report by DDC is not authorized."

(3) "U. S. Government agencies may obtain copies of this report directly from DDC. Other qualified DDC users shall request through _____."

(4) "U. S. military agencies may obtain copies of this report directly from DDC. Other qualified users shall request through _____."

(5) "All distribution of this report is controlled. Qualified DDC users shall request through _____."

If the report has been furnished to the Office of Technical Services, Department of Commerce, for sale to the public, indicate this fact and enter the price, if known.

11. SUPPLEMENTARY NOTES: Use for additional explanatory notes.

12. SPONSORING MILITARY ACTIVITY: Enter the name of the departmental project office or laboratory sponsoring *(paying for)* the research and development. Include address.

13. ABSTRACT: Enter an abstract giving a brief and factual summary of the document indicative of the report, even though it may also appear elsewhere in the body of the technical report. If additional space is required, a continuation sheet shall be attached.

It is highly desirable that the abstract of classified reports be unclassified. Each paragraph of the abstract shall end with an indication of the military security classification of the information in the paragraph, represented as *(TS)*, *(S)*, *(C)*, or *(U)*.

There is no limitation on the length of the abstract. However, the suggested length is from 150 to 225 words.

14. KEY WORDS. Key words are technically meaningful terms or short phrases that characterize a report and may be used as index entries for cataloging the report. Key words must be selected so that no security classification is required. Identifiers, such as equipment model designation, trade name, military project code name, geographic location, may be used as key words but will be followed by an indication of technical context. The assignment of links, rules, and weights is optional.